N 7 1 - 2 5 0 2 8

NASA CR 118311

Plasma Dynamics Laboratory
Technical Report 71-1

April 1971

INSTABILITIES and TURBULENCE in HIGHLY IONIZED PLASMAS in a MAGNETIC FIELD

by J. H. NOON and W. C. JENNINGS

Semi Annual Status Report
NASA Grant No. 33-018-137
September 1, 1970 - February 28, 1971

Electrophysics Division
Rensselaer Polytechnic Institute
Troy, New York

SUMMARY

Further work has been carried out on correlation length and time studies of the plasma turbulence spectrum in the highly ionized argon arc. New probe diagnostics have been developed to allow improved measurements of radial, azimuthal, and axial parameters. The relation between wave growth in different frequency regions of the spectrum and the sense of energy cascade has been studied both experimentally and theoretically. Preliminary results show differences from those of other workers. The technique used can also be applied to determine whether classical or anomalous diffusion across the magnetic field is dominant. An optical diagnostic method has been developed for remote sensing of coherent instabilities and a feedback scheme has been successfully applied to stabilize the plasma against the development of these coherent instabilities. A theoretical analysis shows promise in explaining the underlying mechanisms responsible for wave growth in different radial regions of the inhomogeneous plasma.

INTRODUCTION

This report is concerned with the new results which have been obtained since the last semi-annual status report in October, and results presented at the November meeting of the American Physical Society are not included. This paper was: "Correlation Measurements of Plasma Turbulence Spectra", G. Huchital, J. H. Noon and W. C. Jennings, Bull. Amer. Phys. Soc. 15, 1428 (1970).

The main emphasis in the present study is on the complex interplay and energy exchange between turbulent portions of the observed spectrum and coherent oscillations in the plasma. This is also related to plasma losses across the magnetic field. Although we have the capability of making experimental measurements over a limited range of wave numbers and frequencies, it is clear that in an inhomogeneous plasma in a magnetic field, significant differences can be anticipated in various regions of the plasma.

In addition we have developed new diagnostic techniques and a feedback stabilization scheme. This allows the possibility of controlling turbulence and instability levels without the necessity for altering plasma parameters by external controls such as gas flow rate, magnetic field, etc. A variety of experiments are planned to take advantage of this facility.

All of the work carried out has relevance both to problems of thrustors for manned space flight and to energy generation by plasma means. The techniques used have general applicability.

I. Determination of Diffusion Coefficient by the Diffusion Wave Technique

In the hollow cathode discharge, if charged-particle density perturbations are excited in one region of the plasma by an external source generating a sinusoidal electric field, density waves will diffuse from the point of excitation. These waves are called diffusion waves. By monitoring the amplitude of the density fluctuations and the phase, both the type of diffusion in a magnetic field and the magnitude of the diffusion coefficient can be determined.

This technique was named and first employed by Golubev[1]. His plasmas had a relatively low charged particle density (10^8 - $10^{10}/cm^3$) and were dominated by charged particle-neutral atom collisions at pressures of 0.03 - 1.0 Torr. Golubev's experimental measurements agreed with collisional ambipolar diffusion theory for magnetic fields up to 1500 oersteds. Flannery and Brown[2] used this diffusion wave technique to estimate diffusion rates across the magnetic field in a dense, highly ionized argon plasma where charged particle collisions must be taken into account. They used a hollow cathode discharge similar to the device at Rensselaer. The diffusion waves were excited by superimposing an alternating component on the discharge current. This caused the density perturbation to be applied to the arc core plasma and gave rise to diffusion radially outward from the core. Flannery and Brown's results, (taken over a very small magnetic field range (500 - 550G) appear to indicate that collisional diffusion is the dominant process. They were unable to go beyond this range of magnetic field because the noise level in the plasma increased to the point where measurements of density amplitudes and phases of the diffusion wave were impossible. No mention was made in their report of whether or not coherent oscillations were present, nor was the diffusion coefficient monitored with changes in the level of noise or turbulence.

In the Rensselaer arc we are able to carry out measurements over an increased range of magnetic field (200 - 2200 gauss), by making use of a PAR HR8 lock-in amplifier. In this way it is possible to study both collisional (B^{-2}), and turbulent (B^{-1}) diffusion with and without the presence of large coherent instabilities, while also monitoring the effect of the level of turbulence on the diffusion. We can also extend measurements over a much larger range of magnetic fields, where anomalous plasma transport is more likely to be important.

A. Diffusion Wave Theory

We have developed a theory which represents an extension of that presented by Flannery and Brown, and offers the possibility of examining the effect of turbulence not only upon the type of diffusion across the magnetic field, but also on the way in which energy cascades amongst different frequency components.

The plasma is considered quasi-neutral, ($n_+ = n_-$), and the diffusion wave source is located close to the arc core, allowing the wave to diffuse radially outward. Assuming a radial flux of particles due to diffusion, and using the ion continuity equation, the spatial variation of the diffusion wave in density and phase may be solved for.

The ion continuity equation

$$\frac{\partial n}{\partial t} + \frac{\partial n \langle v_i \rangle}{\partial x_j} = 0 \tag{1}$$

can be written as

$$\frac{\partial \Gamma_z}{\partial z} + \frac{1}{r}\frac{\partial}{\partial r}(r\Gamma_r) + \frac{\partial n}{\partial t} = 0 \tag{2}$$

where Γ_r and Γ_z are the radial and axial fluxes of ions respectively. Adopting the model used by Flannery and Brown, the following assumptions are made:

1. The plasma density and temperature are axially uniform over the length of the arc, L, in the region considered
2. The radial flux of particles, Γ_r, is constant along the axial length of the arc
3. The ions are streaming axially with a directed velocity $V_s \approx (k T_e/m_i)^{1/2}$ *.

With these assumptions equation (2) may be integrated along the axial direction z to yield

$$\Gamma_z\Big|_{z=+\frac{L}{2}} - \Gamma_z\Big|_{z=-\frac{L}{2}} + L\frac{\partial n}{\partial t} + L\frac{1}{r}\frac{\partial}{\partial r}(r\Gamma_r) = 0 \tag{3}$$

where $\Gamma_z\left(\pm\frac{L}{2}\right) = \pm 0.6\, n \left(\frac{kT_e}{m_i}\right)^{1/2}$

---

*This assumption is based on Self and Ewald's[3] theoretical treatment of transport in a one dimensional low pressure discharge. Self and Ewald found that at low pressures the directed plasma velocity near the end walls was the Bohm sheath velocity.

ϵ is an adjustable parameter of the order of unity, to allow for the fact that assumption (3) above may not be entirely correct, and is determined from experimental data.

Therefore

$$\frac{2\epsilon v_s n}{L} + \frac{\partial n}{\partial t} + \frac{1}{r}\frac{\partial}{\partial r}(r\Gamma_r) = 0 \qquad (4)$$

There are two possible cases to consider

a. If the ion diffusion may be described by the rate of anomalous diffusion

$$\Gamma_r \approx -\frac{1}{16B}\frac{\partial}{\partial r}(nT_e) \qquad (5)$$

Here we have changed the original form of the Bohm equation to include the effect of electron temperature gradients.

b. For classical ambipolar diffusion the radial flux may be approximated by

$$\Gamma_r = -\frac{(1.6\times10^{-19})\nu_{ei}}{m_e\omega_e^2}\frac{\partial}{\partial r}\left[n(T_e + T_i)\right] \qquad (6)$$

Where ν_{ei} is the electron-ion collision frequency
ω_e is the electron cyclotron frequency
T_e, T_i is the electron, ion temperature in eV

Equation (6) is strictly valid only for the case of a fully ionized plasma. For the case of a highly ionized discharge it represents a minimum value for radial flux since the effective collision frequency is underestimated.

BOHM DIFFUSION

For the case of Bohm diffusion, equation (4) may be written as

$$\frac{2\epsilon v_s n}{L} + \frac{\partial n}{\partial t} - \frac{1}{16Br}\frac{\partial}{\partial r}\left(r\frac{\partial}{\partial r}nT_e\right) = 0 \qquad (7)$$

We assume that the density is given by $n = n_o + n_1$, where n_o is the static density of ions and n_1 is the density perturbation of the diffusion

wave which is of the form

$$n_1 = N(r)\, e^{i(\vec{k}\cdot\vec{r} - \omega t)} \qquad n_1 \ll n_0 \tag{8}$$

$$\omega = \omega_r \; ; \quad k = k_r \pm f(r) \, , \text{ with N(r) = a real number.}$$

Using this perturbation in equation (7) and taking only the time varying component, yields

$$\frac{2\epsilon V_s}{L} N(r) - i\omega N(r) - \left(\tfrac{1}{16B_r}\right)\left[T_e \frac{\partial N(r)}{\partial r} + ikT_e N(r)\right.$$

$$+ N(r)\frac{\partial T_e}{\partial r} + rT_e \frac{\partial^2 N(r)}{\partial r^2} + 2rT_e ik \frac{\partial N(r)}{\partial r}$$

$$\left. - rT_e k^2 N(r) + 2r \frac{\partial T_e}{\partial r}\frac{\partial N(r)}{\partial r} + 2ikr \frac{\partial T_e}{\partial r} N(r)\right. \tag{9}$$

$$\left. + r N(r) \frac{\partial^2 T_e}{\partial r^2}\right] = 0$$

Setting the imaginary part of this equation = 0

$$\frac{\partial N(r)}{\partial r} + N(r)\left[\frac{1}{T_e}\frac{\partial T_e}{\partial r} + \frac{1}{2r} + \frac{8B\omega}{T_e k}\right] = 0 \tag{10}$$

This can be solved for the radial variation of the amplitude of the perturbation

$$N(r) = \text{Const} \exp -\left[\int^r \left(\frac{1}{T_e}\frac{\partial T_e}{\partial r} + \frac{1}{2r} + \frac{8B\omega}{T_e k}\right) dr\right] \tag{11}$$

Using this result and the real part of equation (9) an equation for k, the wave number of the diffusion wave, can be found

$$k^4 + \left(\frac{32\epsilon V_s B}{T_e L} - \frac{1}{4r^2}\right)k^2 + \left(\frac{8Bw}{T_e^2}\frac{\partial T_e}{\partial r}\right)k - \frac{64B^2\omega^2}{T_e^2} = 0 \qquad (12)$$

Assuming $kr = \phi$, where ϕ = phase shift in radians, we can obtain another equation

$$\phi^4 + \left(\frac{32\epsilon V_s B r^2}{T_e L} - \frac{1}{4}\right)\phi^2 + \left(\frac{8}{T_e^2} Bw \frac{\partial T}{\partial r} r^3\right)\phi - \frac{64 B^2\omega^2 r^4}{T_e^2} = 0 \qquad (13)$$

The diffusion coefficient D_{1B} is given by

$$D_{1B} = \left|\frac{\Gamma_B}{\partial n/\partial r}\right|_{\frac{\partial T_e}{\partial r}=0} \qquad (14)$$

CLASSICAL DIFFUSION

The same calculations can be performed for the case of classical diffusion using equations (4) and (6). From this we find

$$N(r) \simeq \text{Const} \exp -\left[\int\left(\frac{\omega T_e^{1/2}}{2C n_0 k} + \frac{1}{2r} + \frac{T_e^{1/2}}{2}\frac{\partial T_e^{-3/2}}{\partial r} + \frac{3}{2T_e}\frac{\partial T_e}{\partial r}\right)dr\right] \qquad (15)$$

and

$$\phi^4 C n_0 T_e^{-1/2} + \phi^2\left(\frac{2\epsilon V_s}{L} r^2\right) + \phi^2 r^2 C n_0\left(-\frac{1}{2r T_e^{1/2}}\frac{\partial T}{\partial r}\right. \qquad (16)$$

$$\left. - \frac{1}{2} T_e^{1/2}\frac{\partial^2 T_e}{\partial r^2} + \frac{9}{4 T_e^{1/2}}\left(\frac{\partial T_e}{\partial r}\right)^2\right) + \phi\left(\frac{r^2\omega}{2T_e^{1/2}}\frac{\partial T_e^{1/2}}{\partial r}\right) - \frac{\omega^2 r^4}{4 C n_0 T_e^{-1/2}} = 0$$

Where we have assumed $T_e >> T_i$ and $\nu_{ei} = \text{Const } n\, T_e^{-3/2}$ and $C = \dfrac{\text{Const } e}{m_e \omega_e^2}$

The diffusion coefficient is given by

$$D_{\perp cl} = \left. \frac{|\Gamma_{cl}|}{|\partial n/\partial r|} \right|_{\frac{\partial T_e}{\partial r} = 0} \qquad (17)$$

USING THEORETICAL PREDICTIONS

In order to be able to fit the theory to experimental results for k or ϕ, a digital computer solution is required. The quantities ϵ and $D_\perp$ serve as adjustable parameters in the theory, but a unique solution requires fixing both quantities.

In practice, temperature and density profiles are determined by Langmuir probe measurements in the plasma. In order to see the different effects classical and Bohm diffusion have on the propagation of a diffusion wave, sample density and temperature profiles representing typical arc conditions were taken, (see Fig. 1), and fed into the digital computer to predict the propagation of the diffusion wave. It can be seen that for both Bohm and classical (Figs. 2 and 3) diffusion, the propagation of the diffusion wave is greatly affected by both the magnetic field strength and the frequency of the wave itself. It also can be seen that for a given frequency diffusion wave Bohm and classical diffusion theory predict vastly different propagation characteristics.

THE EXPERIMENT

The diffusion wave is fed into the plasma by placing an alternating voltage on a Langmuir probe positioned at the edge of the arc core. The density amplitude and phase of the wave is detected by another Langmuir probe which is radially movable in the same plane as the feeder probe. To measure the density amplitude the resulting probe signal is fed into a Hewlett Packard model 310 wave analyzer. The phase of the wave is determined by feeding the probe signal into a PAR model HR 8 lock-in amplifier. These measurements are being performed at this time. The use of the high sensitivity lock-in amplifier should increase the range of magnetic field strength that this technique is applicable to, thus making it possible to observe changes in the magnitude of the

diffusion coefficient and the change from classical to anomalous diffusion with changes in the level of turbulence and the onset of large coherent instabilities such as the drift wave and ion acoustic wave previously reported[3].

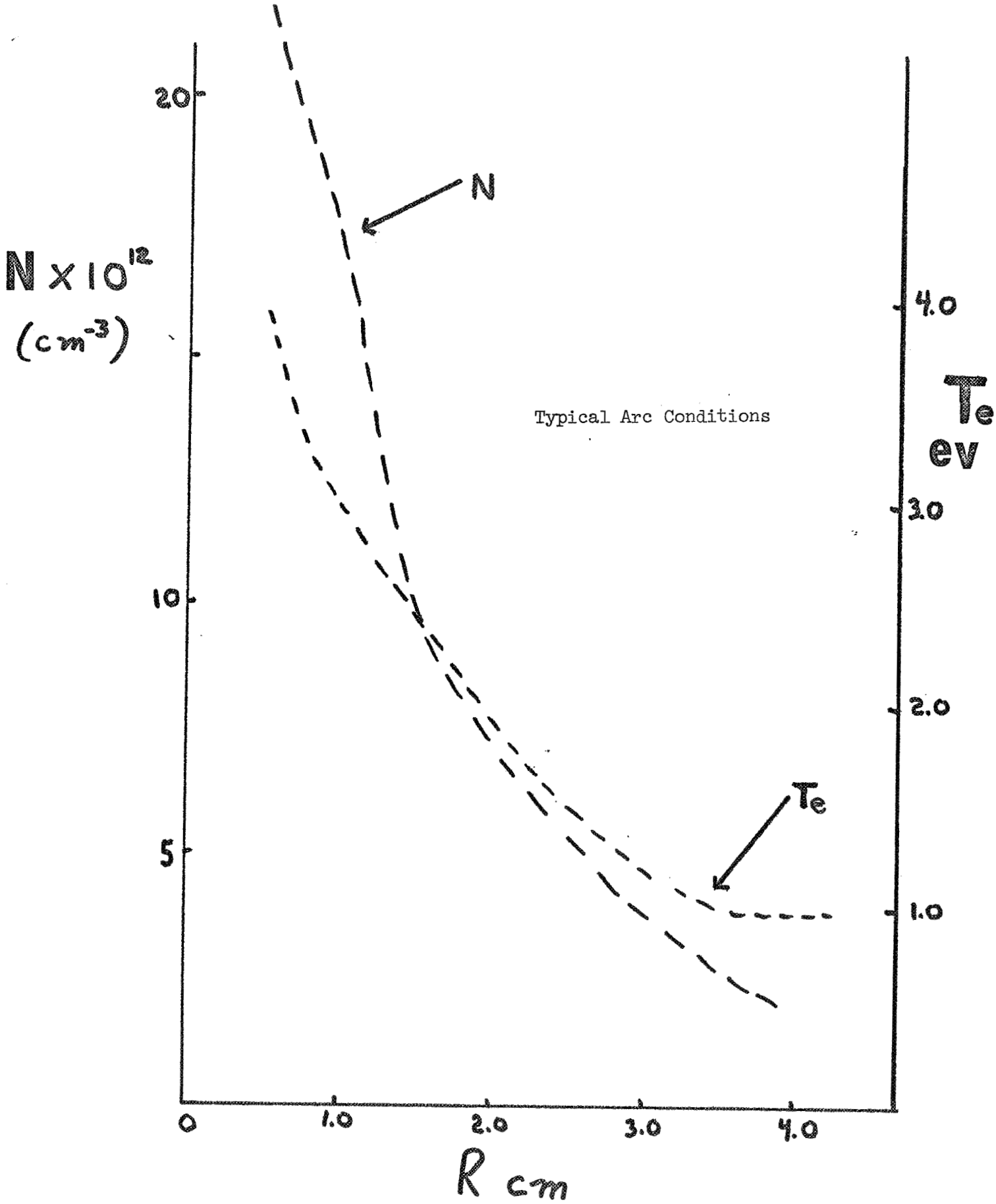
N x 10^12
(cm^-3)
20
10
5
N
Typical Arc Conditions
Te
ev
4.0
3.0
2.0
1.0
Te
0
1.0
2.0
3.0
4.0
R cm

Fig 1

Phase Shift vs. distance from arc core; B = 350 G, ◆ ;
B = 1500 G, ▲ , Classical Diffusion ω = 6 KHz; ○ , B = 350 G,
□ , B = 1500 G Bohm Diffusion ω = 60 KHz

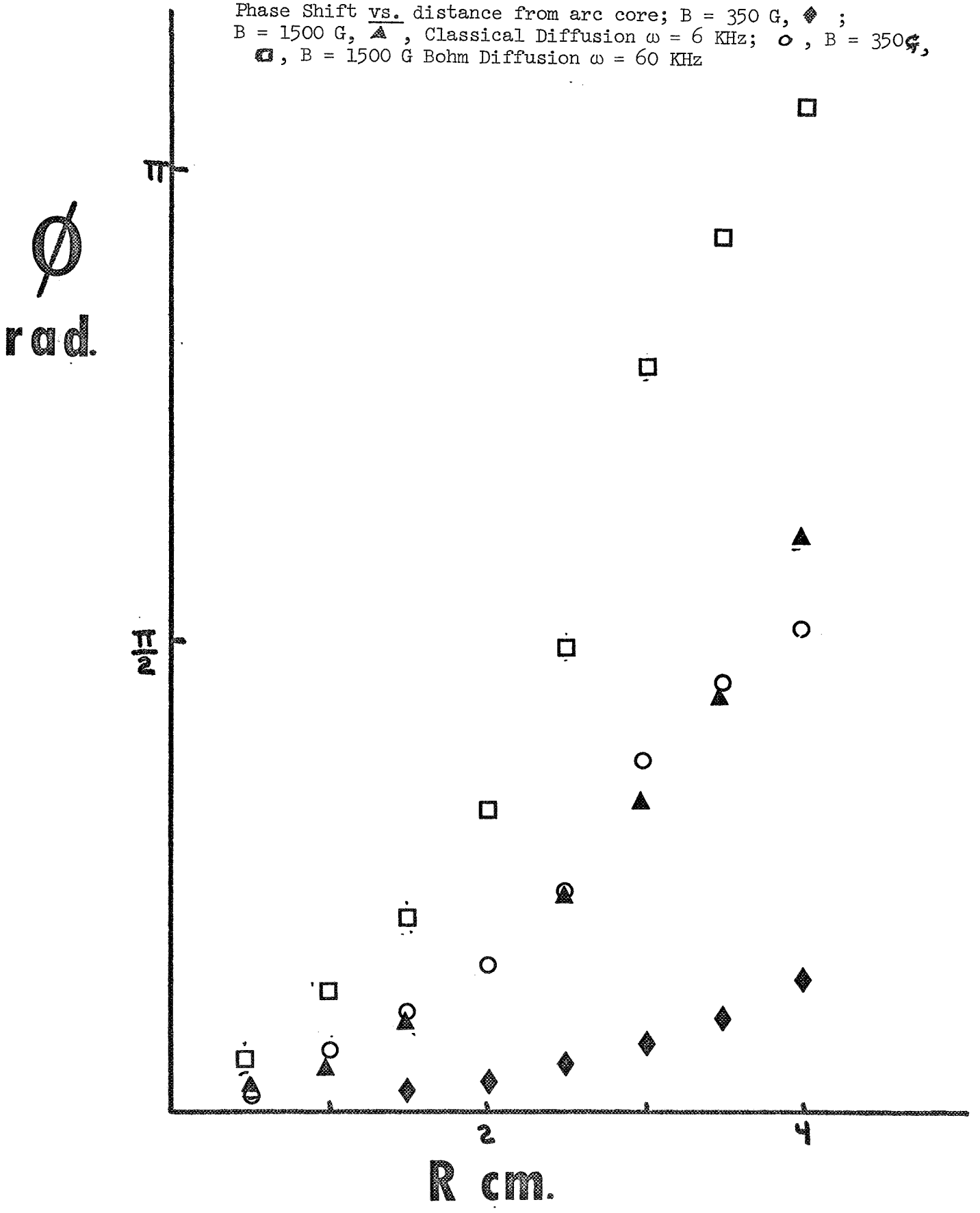

Fig 2

Phase Shift of Diffusion Wave vs. distance from arc core; ♦ 6 KHz, ▲ 30 KHz for Bohm Diffusion; ○ 6 KHz; □ 30 KHz for Classical Diffusion; B = 890 G

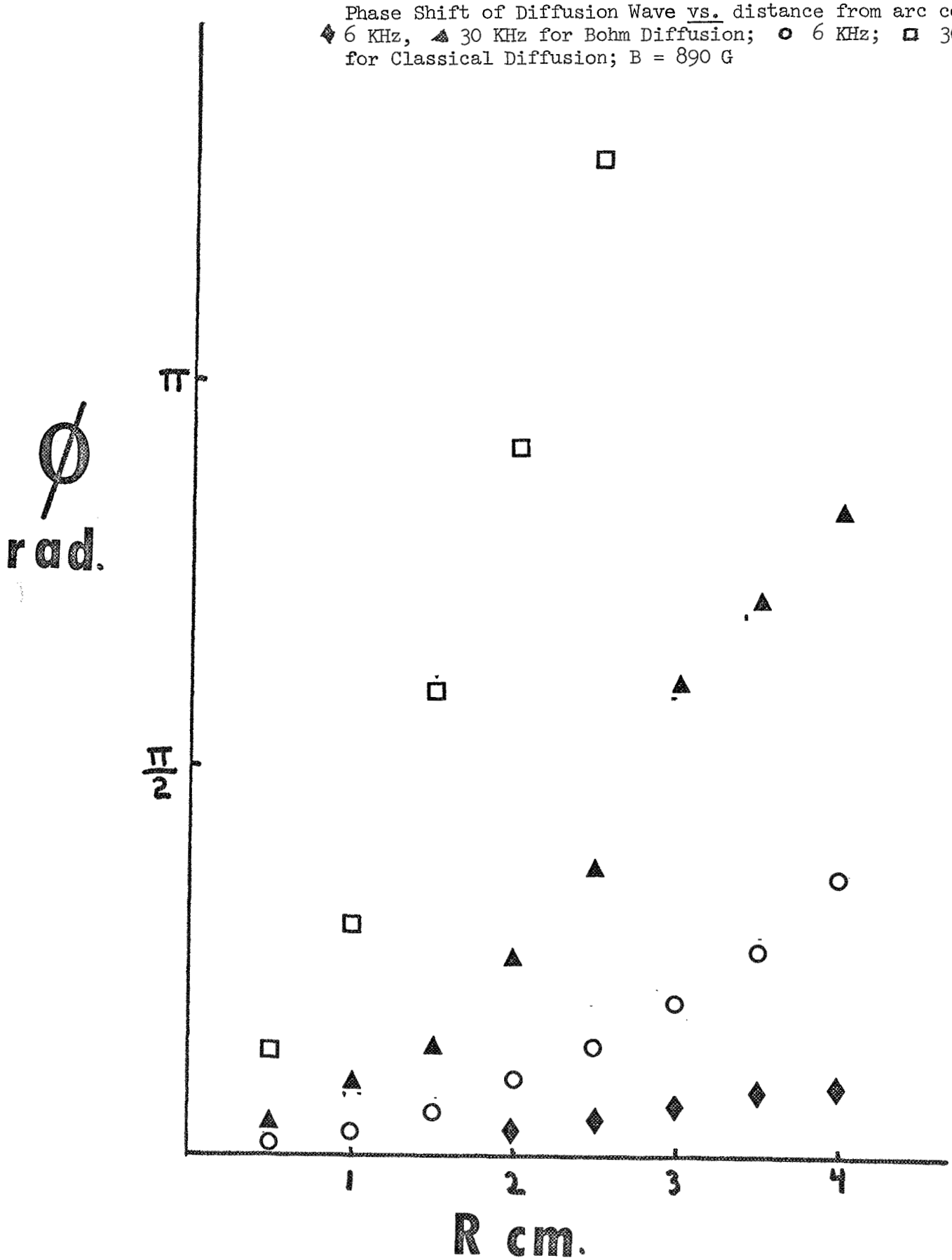

Fig 3

II. Wave Wave-Interaction

Nonlinear interaction between different waves in a plasma has been considered by several authors[5-10]. It is found that if the wave numbers and frequencies of three waves satisfy the condition $k_1 + k_2 = k_3$ and $\omega_1 + \omega_2 = \omega_3$, the amplitudes of the three waves are coupled under the condition of classical diffusion. If Bohm diffusion is assumed, no coupling between the waves is evident. This can be seen by examining the two basic equations of the last section.

For the case where we assume Bohm diffusion, using the continuity equation we have

$$\frac{2\epsilon V_s n}{L} + \frac{\partial n}{\partial t} - \frac{1}{16Br}\left[T_e \frac{\partial n}{\partial r} + n\frac{\partial T_e}{\partial r} + r T_e \frac{\partial^2 n}{\partial r^2}\right. \tag{II-1}$$
$$\left. + 2r \frac{\partial n}{\partial r}\frac{\partial T_e}{\partial r} + nr\frac{\partial^2 T_e}{\partial r^2}\right] = 0$$

For classical diffusion

$$\frac{2\epsilon V_s n}{L} + \frac{\partial n}{\partial t} - \frac{c}{r} n T^{-1/2}\frac{\partial n}{\partial r} - \frac{c}{r} n^2 T^{-3/2}\frac{\partial T}{\partial r}$$
$$- cnT\frac{\partial T^{-3/2}}{\partial r}\frac{\partial n}{\partial r} - cn^2\frac{\partial T^{-3/2}}{\partial r}\frac{\partial T}{\partial r} - cT^{-1/2}\frac{\partial n}{\partial r}\frac{\partial n}{\partial r} \tag{II-2}$$
$$- cnT^{-1/2}\frac{\partial^2 n}{\partial r^2} - 3cnT^{-3/2}\frac{\partial T}{\partial r}\frac{\partial n}{\partial r} - cn^2 T^{-3/2}\frac{\partial^2 T}{\partial r^2} = 0$$

Assuming a density $n = n_o + n_p$ where n_p is the density perturbation and $n_o \gg n_p$, only the equation related to classical diffusion will be non-linear in the density n. Thus if we assume the perturbed density is of the form

$$n_p = \sum_{j=1}^{J} n_j \tag{II-3}$$

where

$$n_j = \tfrac{1}{2}\left(N_j(r)\, a_j(t)\, e^{i\psi_j} + N_j^*(r)\, a_j^*(t)\, e^{-i\psi_j}\right) \tag{II-4}$$

$\Psi_j = K_j r - W_j I$ K = real constant

$K_3 = K_1 + K_2$ W = real constant

$W_3 = W_1 + W_2$

Equation II-1 will exhibit no coupling between the three perturbations n_1, n_2 and n_3, whereas the classical diffusion equation (II-2) will couple the d.c. density n_o along with n_1, n_2 and n_3.

The usual notation for a perturbation in density is $n \propto e^{(kr - \omega t)} + c.c.$ If we let k and ω both be complex quantities with $k_r = K + k_r(r)$ and $\omega_r = W + \omega_r(t)$ the perturbation can be written in the form

$$\eta = e^{iKr} e^{ik_r(r)\cdot r} e^{+ik_I(r)\cdot r} e^{-iWt} e^{-i\omega_r(t)\tau} e^{i\omega_r \tau} + c.c. \quad \text{(II-5)}$$

If we let $N(r) \propto e^{i k_r(r) \cdot r} e^{+ k_I \cdot r}$ and $a(t) \alpha e^{-iw_r(t)} e^{+w_I(t) t}$ the perturbation can be written in the form of equation II-4.

Inserting equation II-4 into equation II-2 we end up with an equation of the form

$$\begin{aligned}
&[A(r,\tau) + i B(r,\tau)] e^{i\Psi_1} + [C(r,\tau) + i D(r,\tau)] e^{i\Psi_2} \\
&+ [E(r,\tau) + i F(r,\tau)] e^{i\Psi_3} + [G(r,\tau) + i H(r,\tau)] e^{i(2\Psi_1 + \Psi_2)} \\
&+ [I(r,\tau) + i J(r,\tau)] e^{i(\Psi_1 + 2\Psi_2)} + [K(r,\tau) + i L(r,\tau)] e^{i 2\Psi_1} \\
&+ [M(r,\tau) + i N(r,\tau)] e^{i 2\Psi_2} + [O(r,\tau) + i P(r,\tau)] e^{i 2\Psi_3} \\
&+ [Q(r,\tau) + i R(r,\tau)] = 0
\end{aligned} \quad \text{(II-6)}$$

One possible solution to this equation can be found by setting all coefficients of $e^{i\psi} = 0$. Therefore

$$A(r, t) + i\, B(r, t) = 0$$

or

$$A(r, t) = 0 \quad ; \quad B(r, t) = 0$$

For this case if we let N(r) be real

$$A(r,\tau) + i\,B(r,\tau) = \frac{2\sigma\nu_s}{L} N_1(r)\, a_1(\tau) + N_1(r)\frac{\partial a_1(\tau)}{\partial \tau}$$

$$+ a_1(\tau)\left[-A m_0 \frac{\partial N_1}{\partial r} - 2B m_0 N_1 - F\left(2\frac{\partial m_0}{\partial r}\frac{\partial N_1}{\partial r} - K_1^2 N_1 m_0 + m_0 \frac{\partial^2 N_1}{\partial r^2}\right)\right]$$

$$- a_2^*(\tau)\, a_3(\tau)\left[-A\left(N_3\frac{\partial N_2}{\partial r} + N_2\frac{\partial N_3}{\partial r}\right) - 2B N_2 N_3\right.$$

$$\left. - F\left(\frac{\partial N_3}{\partial r}\frac{\partial N_2}{\partial r} + K_2 K_3 N_2 N_3 - K_3^2 N_2 N_3 + N_2\frac{\partial^2 N_3}{\partial r^2} - K_2^2 N_3 N_2 + N_3\frac{\partial^2 N_2}{\partial r^2}\right)\right] \qquad \text{(II-7)}$$

$$+ i\, a_1(\tau)\left[-A m_0 K_1 N_1 - F\left(2\frac{\partial m_0}{\partial r} K_1 N_1 + 2K_1\frac{\partial N_1}{\partial r} m_0\right)\right]$$

$$+ i\, a_2^*(\tau)\, a_3(\tau)\left[-A\left(-K_2 N_3 N_2 + K_3 N_3 N_3\right)\right.$$

$$\left. - F\left(-K_2\frac{\partial N_3}{\partial r} N_2 + K_3 N_3\frac{\partial N_2}{\partial r} + 2N_2 K_3\frac{\partial N_3}{\partial r} - 2K_2 N_3\frac{\partial N_3}{\partial r}\right)\right]$$

where $$A = C\left(\frac{1}{\rho T^{1/2}} + \frac{T}{\partial r}\frac{\partial T^{-3/2}}{\partial r} + 3T^{-3/2}\frac{\partial T}{\partial r}\right)$$

$$B = C\left(\frac{1}{\rho T^{1/2}}\frac{\partial T}{\partial r} + \frac{\partial T^{-3/2}}{\partial r}\frac{\partial T}{\partial r} + T^{-3/2}\frac{\partial^2 T}{\partial r^2}\right)$$

and $$F = \frac{C}{T^{1/2}}$$

Writing $a_j(t) = |a_j(t)|\, e^{i\phi_j}$, the imaginary part of equation II-7 becomes

$$|a_1(t)|\left[N_1\frac{\partial \phi_1}{\partial t} - A m_0 K_1 N_1 - F\left(2\frac{\partial m_0}{\partial r}K_1 N_1 + 2K_1\frac{\partial N_1}{\partial r}m_0\right)\right]$$

$$+ |a_1(t)||a_3(t)|\cos\Phi\left[-A(K_3 N_1 N_3 - K_1 N_1 N_1)\right.$$

$$\left. - F\left(-K_1\frac{\partial N_3}{\partial r}N_1 + K_3 N_3\frac{\partial N_1}{\partial r} + 2K_3 N_1\frac{\partial N_3}{\partial r} - 2K_1 N_3\frac{\partial N_1}{\partial r}\right)\right]$$

$$+ |a_2(t)||a_3(t)|\left[-A\left(N_3\frac{\partial \omega_2}{\partial r} + N_2\frac{\partial \omega_3}{\partial r}\right)\right. \qquad \text{(II-8)}$$

$$- 2\beta N_2 N_3 - F\left(\frac{\partial N_3}{\partial r}\frac{\partial \omega_2}{\partial r} + K_2 K_3 N_2 N_3 - K_3^2 N_2 N_3\right.$$

$$\left.\left. + \omega_2\frac{\partial^2 N_3}{\partial r^2} - K_2^2 N_3 N_2 + N_3\frac{\partial^2 N_2}{\partial r^2}\right)\right]\sin\Phi = 0$$

The real part of equation II-7 is

$$N_1 \frac{\partial |a_1(r)|}{\partial \tau} + |a_1| \left[\frac{2\epsilon V_1}{L} N_1 - A m_0 \frac{\partial N_1}{\partial r} - 2B m_0 N_1 - F\left(2 \frac{\partial m_0}{\partial r} \frac{\partial N_1}{\partial r} - K_1^2 N_1 m_0 + m_0 \frac{\partial^2 N_1}{\partial r^2} \right) \right]$$

$$+ |a_2||a_3| \cos\Phi \left[-A\left(N_3 \frac{\partial N_2}{\partial r} + N_2 \frac{\partial N_3}{\partial r} \right) - 2B N_2 N_3 \right. \qquad \text{(II-9)}$$

$$- F\left(\frac{\partial N_2}{\partial r} \frac{\partial N_3}{\partial r} + K_2 K_3 N_3 N_2 - K_3^2 N_2 N_3 + N_2 \frac{\partial^2 N_3}{\partial r^2} - K_2^2 N_3 N_2 \right.$$

$$\left. \left. + N_3 \frac{\partial^2 N_2}{\partial r^2} \right) \right]$$

$$- |a_2||a_3| \sin\Phi \left[-A\left(-K_2 N_3 N_2 + K_3 N_2 N_3 \right) \right.$$

$$\left. - F\left(-K_2 \frac{\partial N_3}{\partial r} N_2 + K_3 N_3 \frac{\partial N_2}{\partial r} + 2K_3 N_2 \frac{\partial N_3}{\partial r} - 2K_2 N_3 \frac{\partial N_2}{\partial r} \right) \right] = C$$

or

$$N_1 \frac{\partial |a_1|}{\partial \tau} + |a_1| [A_1] + |a_2||a_3| \cos\Phi [B_1] \qquad \text{(II-10)}$$

$$- |a_2||a_3| \sin\Phi [C_1] = 0$$

and

$$|a_1| \left[N_1 \frac{\partial \phi_1}{\partial \tau} + A_1 \right] + |a_2||a_3| \cos\Phi [C_1]$$

$$+ |a_2||a_3| \sin\Phi [B_1] = 0 \qquad \text{(II-11)}$$

where A_1, B_1 and C_1 are the appropriate terms in brackets in equation II-9 or II-8.

Similarly for the coefficients of $e^{i\Psi_2}$ (equation II-6)

$$N_2 \frac{\partial |a_2|}{\partial t} + |a_2| [A_2] + |a_1||a_3| \cos\Phi [B_2] - |a_1||a_3| \sin\Phi [C_2] = 0 \qquad \text{(II-12)}$$

and

$$|a_2| \left[N_2 \frac{\partial \phi_2}{\partial t} + A_2 \right] + |a_1||a_3| \cos\Phi [C_2] + |a_1||a_3| \sin\Phi [B_2] = 0 \qquad \text{(II-13)}$$

where in equations II 12, 13 A_2, B_2, C_2 replace the equivalent terms A_1, B_1, C_1 in equations II 10, 11 with the subscripts 1 and 2 interchanged.

Also for the coefficients of $e^{i\Psi_3}$

$$N_3 \frac{\partial |a_3|}{\partial t} + |a_3| X_1 + |a_1||a_2| \cos\Phi X_2 + |a_1||a_2| \sin\Phi X_3 = 0 \qquad \text{(II-14)}$$

and

$$|a_3| \frac{\partial \phi_3}{\partial t} + |a_3| X_4 - |a_1||a_2| \sin\Phi X_3 + |a_1||a_2| \cos\Phi X_2 = 0 \qquad \text{(II-15)}$$

where

$$X_1 \approx \frac{2\epsilon V_3}{L} N_3 - A m_0 \frac{\partial N_3}{\partial r} - 2B m_0 N_3$$

$$X_2 = - A\left(N_1 \frac{\partial N_2}{\partial r} + N_2 \frac{\partial N_1}{\partial r}\right) - 2B N_1 N_2$$

$$- F\left(2 \frac{\partial N_2}{\partial r} \frac{\partial N_1}{\partial r} - 2 K_1 K_2 N_2 N_1 - K_2^2 N_1 N_2 + N_1 \frac{\partial^2 N_2}{\partial r^2}\right.$$

$$\left. - K_1^2 N_2 N_1 + N_2 \frac{\partial^2 N_1}{\partial r^2}\right)$$

$$X_3 = - A\left(K_2 N_1 N_2 + K_1 N_2 N_1\right) - F\left(2 K_1 \frac{\partial N_2}{\partial r} N_1\right.$$

$$\left. + 2 K_2 N_2 \frac{\partial N_1}{\partial r} + 2 N_1 K_2 \frac{\partial N_2}{\partial r} + 2 N_2 K_1 \frac{\partial N_1}{\partial r}\right)$$

and $$X_4 = - \omega_3 N_3 - A m_0 K_3 N_3$$

$$- F\left(2 \frac{\partial m_0}{\partial r} K_3 N_3 + 2 m_0 K_3 \frac{\partial N_3}{\partial r}\right) \qquad \text{(II-16)}$$

If we assume that the third wave is initially absent ($a_3(0) = 0$) and $\Phi = \phi_3 - \phi_2 - \phi_1 = 0$, the real parts of these equations can be written in Laplace transform form as

$$s|a_1| = -|a_1| \frac{A_1}{N_1} - |a_2||a_3| \frac{B_1}{N_1}$$

$$s|a_2| = -|a_2| \frac{A_2}{N_2} - |a_1||a_3| \frac{B_2}{N_2} \qquad \text{(II-17)}$$

$$s|a_3| = -|a_3| \frac{X_1}{N_3} - |a_1||a_2| \frac{X_2}{N_3}$$

Eliminating a_2 from the above equations

$$|a_3|^2\left(s+\frac{X_1}{N_3}\right)=|a_1|^2\left(s+\frac{A_1}{N_1}\right)\frac{N_1}{B_1}\frac{X_2}{N_3} \qquad \text{(II-18)}$$

or eliminating a_1

$$|a_3|^2\left(s+\frac{X_1}{N_3}\right)=|a_2|^2\left(s+\frac{A_2}{N_2}\right)\frac{X_2 N_2}{N_3 B_2} \qquad \text{(II-19)}$$

To a first approximation,

$$\frac{x_1}{N_3}\doteq\frac{A_1}{N_1}\doteq\frac{A_2}{N_2}$$

therefore

$$\begin{aligned} B_1 N_3|a_3|^2-N_1 X_2|a_1|^2 &= \text{CONST}=|a_{10}|^2 \\ N_3 B_2|a_3|^2-N_2 X_2|a_2|^2 &= \text{CONST}=|a_{20}|^2 \end{aligned} \qquad \text{(II-20)}$$

where $|a_{10}|$ and $|a_{20}|$ are the initial values of waves 1 and 2. Thus we can see that the time dependence of the three waves are directly coupled to each other.

Solving equations II-17 and II-20 for $|a_3|$ we find

$$\left(\frac{d|a_3|}{d\tau}\right)^2=-\frac{|a_3|^4 B_1 B_2 N_3^2}{N_1 N_2^2}-|a_3|^2\left(\frac{X_1^2}{N_3^2}-\frac{B_1 N_3}{N_1 X_2}|a_{20}|^2-\frac{N_3 B_2}{X_2 N_2}|a_{10}|^2\right)-|a_{10}|^2|a_{20}|^2 \qquad \text{(II-21)}$$

Equations of this form were derived by Das[5] using the continuity and momentum equations for electrons along with Maxwell's equations. He was able to solve equation II-21 and similar equations for $|a_2|$ and $|a_1|$ to show that the energy is being periodically exchanged among the three waves in an energy transfer cycle. Under a specific set of conditions this transfer of energy will go only in one direction. The third wave begins to grow continually and the first two wave gradually die out.

This technique may be used to explain some of the three wave interactions we observe in the Rensselaer hollow cathode discharge, but its importance may lie in extending the perturbations to include turbulent oscillations.

Assuming a perturbation of the form

$$n_j = \sum_{j=1}^{\infty} N_j a_j e^{i\psi_j} + c.c.$$

coupled equations of the form

$$\frac{d|a_1}{d\tau} = \gamma_1 a_1 + \gamma_2 a_1^* a_3 + \gamma_3 a_4^* a_5 + \cdots$$

$$\frac{d|a_2}{d\tau} = \gamma_1 a_2 + \gamma_2 a_1^* a_3 + \cdots$$

$$\vdots$$

can be found which may be used to explain the cascade of energy amongst different frequency components in a turbulent plasma.

III. Experiment

Examples of the wave-wave interaction process can be seen in our plasma by externally exciting a diffusion wave (see Section 1) in the presence of a large coherent oscillation. Figure 4 shows the interaction of a diffusion wave at 60 KHz with a 4 KHz ion acoustic wave and its harmonics. Both sum and difference frequency waves are excited ($\omega_{DW} \pm \omega_{IAW}$, $\omega_{DW} \pm \omega_{Harmonics}$). The same effect can be seen for the interaction of a diffusion wave and a 5 KHz drift wave (Fig. 5), but in this case no harmonics of the drift wave were present. Sum and difference frequencies were generated at $\omega_{DW} \pm \omega_d$ and only the sum frequency at $\omega_{DW} + 2\,\omega_d$. The difference frequency $\omega_{DW} - 2\,\omega_d$ may be lost in the noise since no correlation techniques was used to attempt to separate it out.

Wave interactions like this do not always occur for all radial positions in the arc. In Fig. 6 the diffusion wave at 60 KHz is interacting with an ion acoustic wave and its harmonics. It appears that only sum frequencies are generated. At the same time, the diffusion wave interacts with a small oscillation located at 25KHz causing it to decrease in amplitude and almost become lost in the noise.

Fig. 7 was taken at a radial position where no large harmonics of the ion acoustic wave were present, and in this case the application of the diffusion wave feeds energy into a broad range of frequencies around 25 KHz without affecting the ion acoustic wave or its harmonics significantly. These effects can be seen for a large range of diffusion wave frequencies (25 KHz - 100 KHz at least). Work is being carried out at this time to determine exactly what plasma conditions are influencing the wave-wave interactions which occur.

If the data of Fig. 7 is studied on a graph with an expanded amplitude axis it can be seen that the energy of the diffusion wave is being coupled out both up and down the frequency spectrum. This is contrary to what was found by Roth[11] who observed a cascade of energy only from low frequencies to higher frequencies. These differences may be reconciled by a theory based on wave-wave interactions as described in the last section. Quantitative predictions, however, are not possible at the present time.

The cascade of energy in both directions can be seen more clearly under different operating conditions where any coherent oscillations that are present are smaller than the ion acoustic or drift waves discussed previously. Figure 8 shows clearly that the energy from the diffusion wave is cascading in both directions, with most of the energy going into those frequency components close to the diffusion wave frequency. The low frequency portion of the spectrum is also affected. The noise level seems to rise slightly, while the coherent oscillation is shifted in frequency. Again at different positions in the plasma the direction of cascade is not constant. At a different radius, (Fig. 9), only the part of the spectrum near the wave is affected by the excitation of the diffusion wave. Changing

the magnetic field also causes a different effect, as in Fig. 10, where the addition of the diffusion wave has no effect on the turbulent spectrum.

At this time it has not been possible to correlate the different types of energy cascade observed with changing plasma conditions but work is continuing on this topic. It seems likely that the wave-wave interaction theory described in the last section can be used to explain observed phenomena.

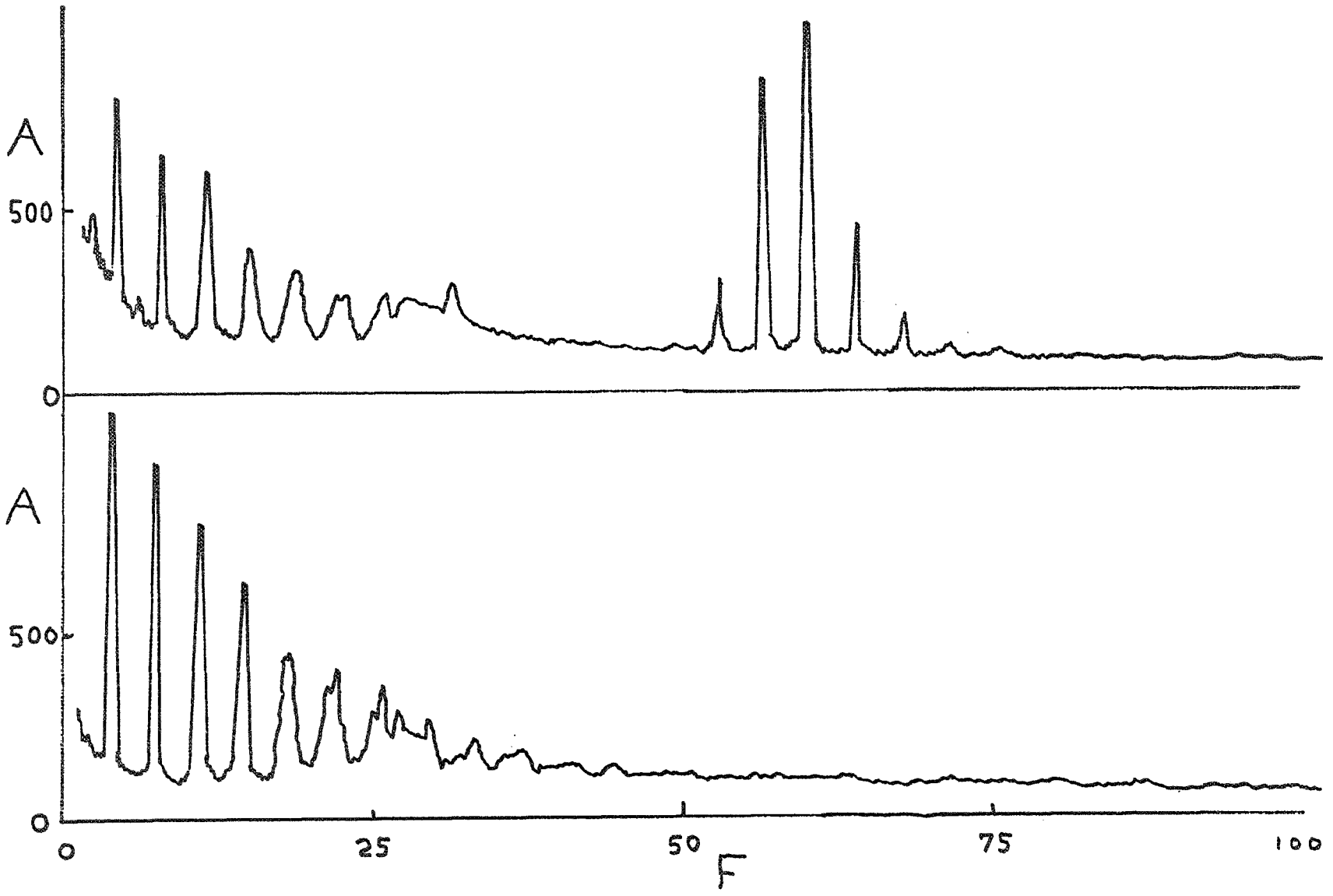

Amplitude vs. Frequency, 0 - 100 KHz; ion acoustic wave (and harmonics) at 4 KHz, B = 680 G, I_{arc} = 20A, V_{arc} =42 V. Lower curve, no diffusion wave. Upper curve, diffusion wave at 4.5 cm from arc core showing applied 60 KHz plus sum and difference frequencies excited.

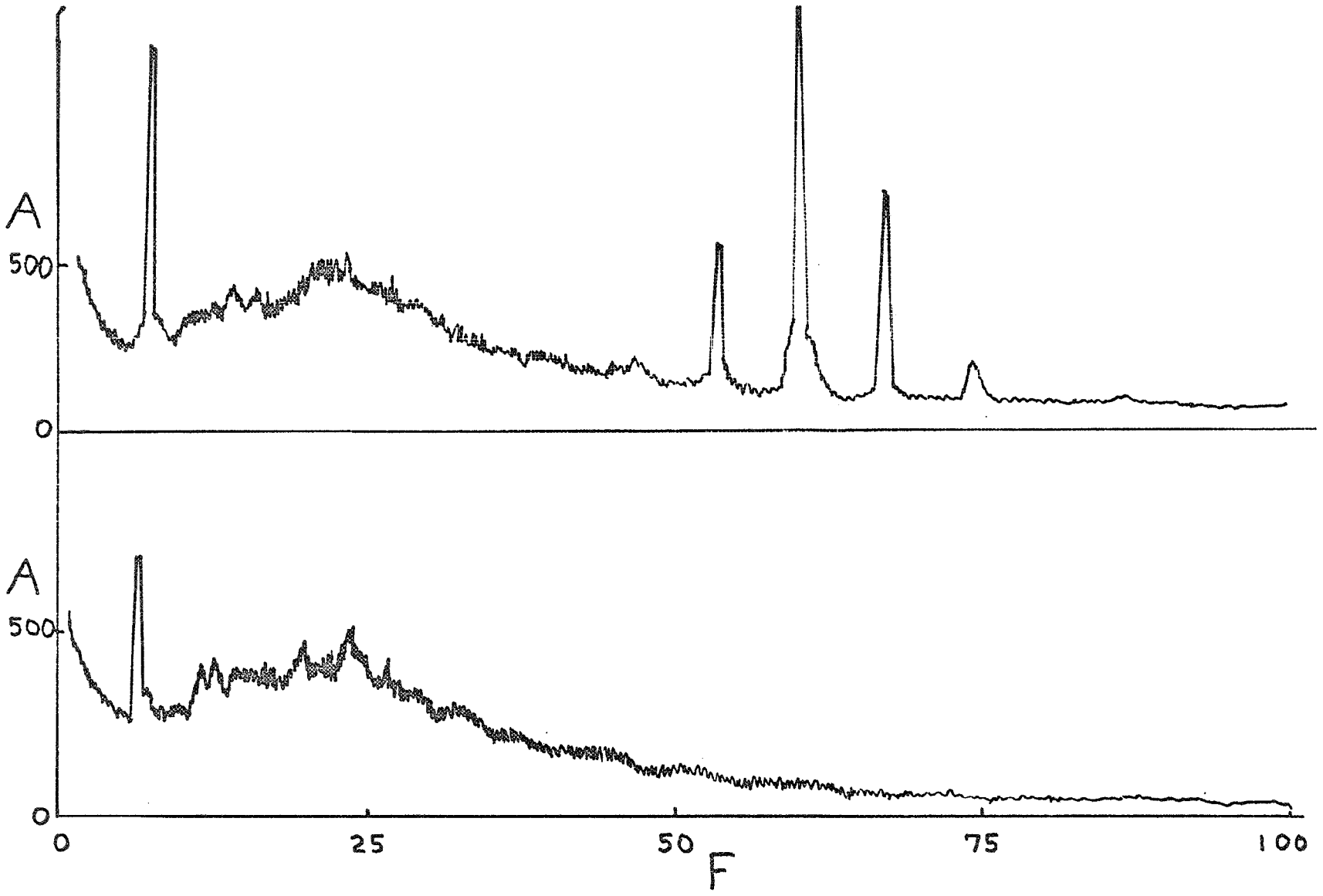

Amplitude vs. Frequency 0 - 100 KHz; drift wave present at 7 KHz, B = 1200 G, I_{arc} =19A, V_{arc} = 43 V. Lower curve, no diffusion wave. Upper curve, diffusion wave at 2.5 cm from arc core showing applied 60 KHz plus sum and difference frequencies excited.

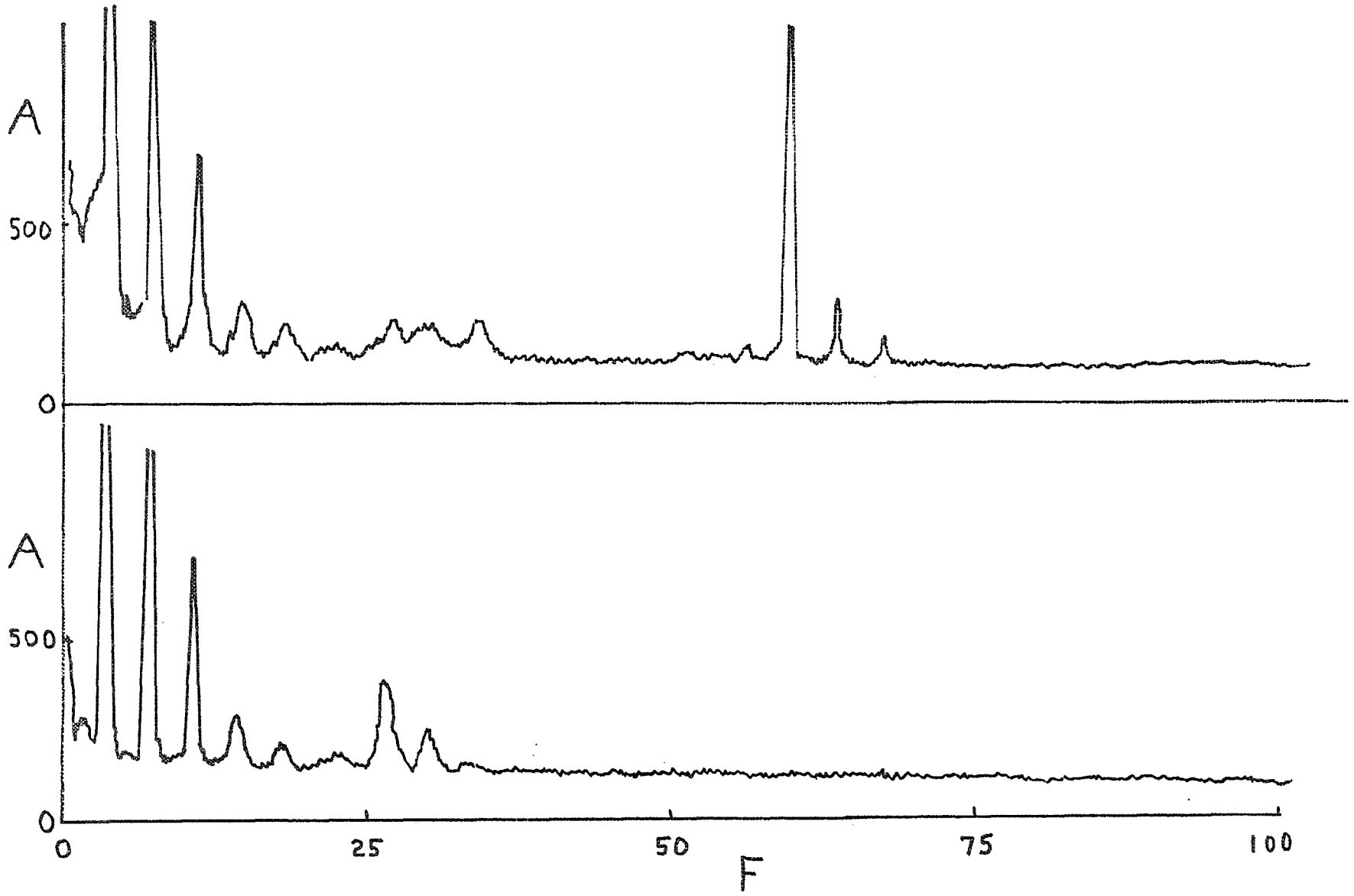

Amplitude vs. Frequency, 0 - 100 KHz; ion acoustic wave present at 4 KHz, B = 680 G, I_{arc} = 20A, V_{arc} =42 V. Lower curve, no diffusion wave. Upper curve, diffusion wave at 2.5 cm from arc core showing applied 60 KHz but only sum frequencies excited.

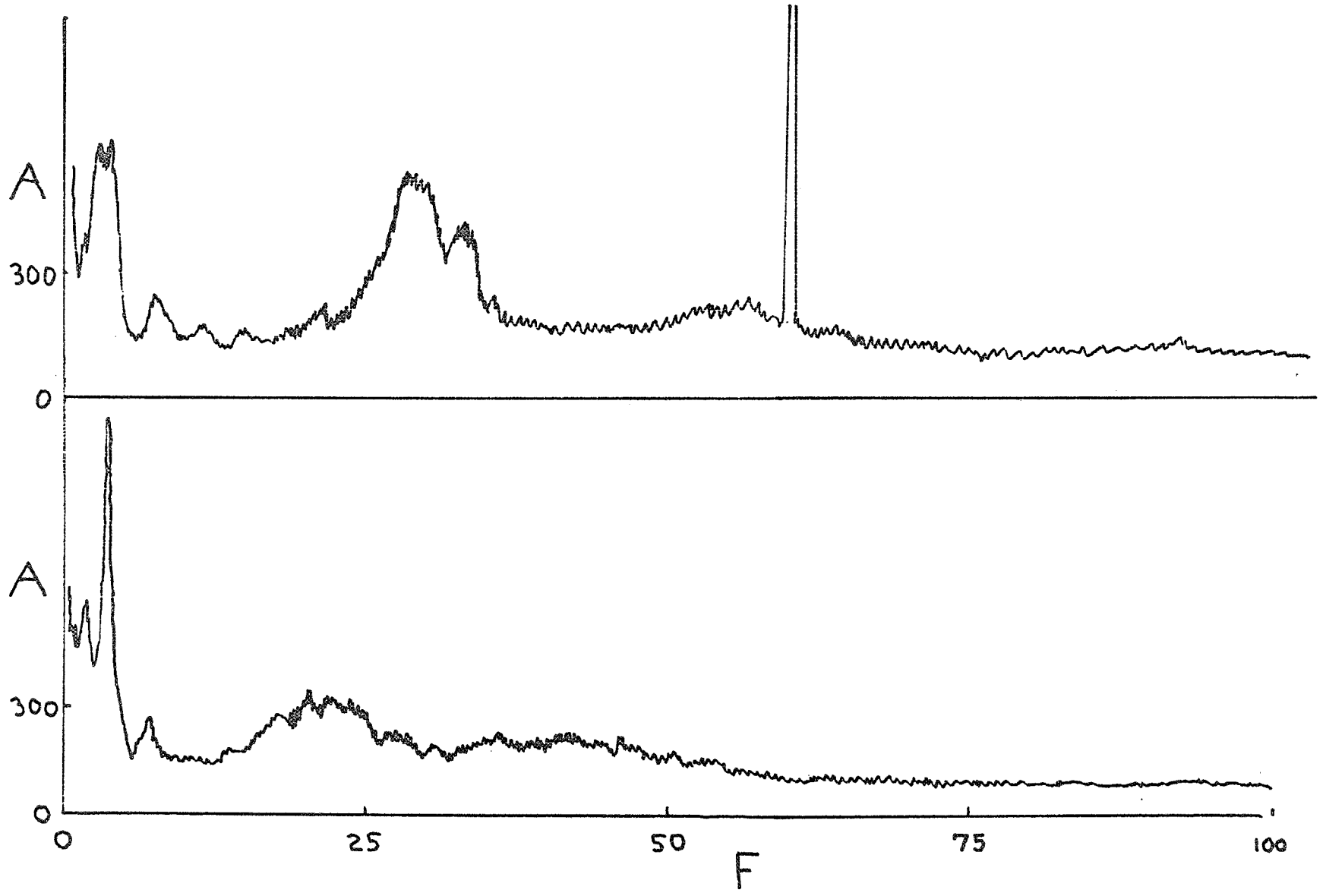

Amplitude vs. Frequency, 0 - 100 KHz; ion acoustic wave present at 4 KHz. B = 680 G, I_{arc} = 20A, V_{arc} = 42 V. Lower curve, no diffusion wave. Upper curve, diffusion wave at 1 cm from arc core showing applied 60 KHz causes only slight enhancement throughout the turbulent spectrum.

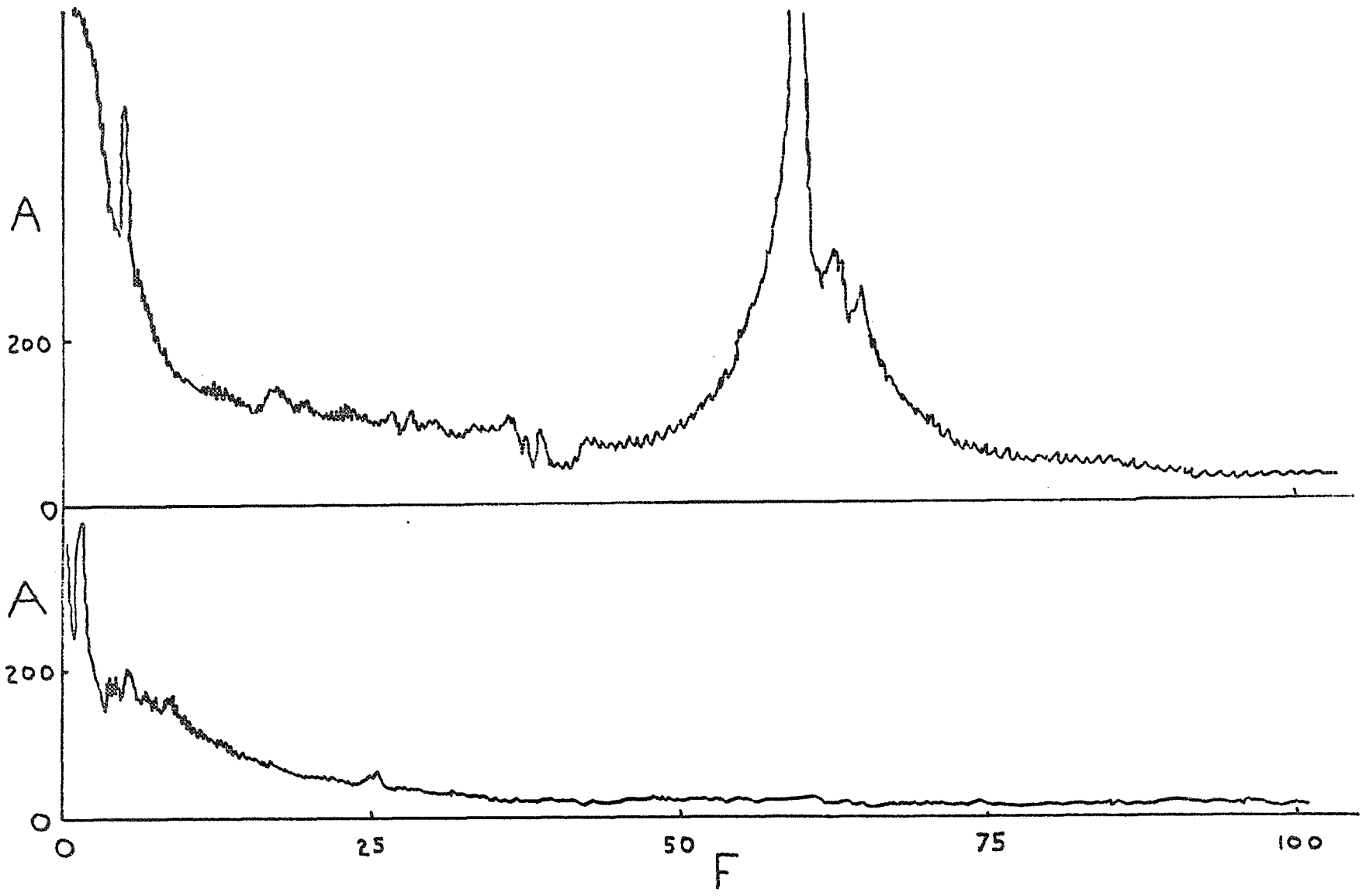

Amplitude vs. Frequency, 0 - 100 KHz; No coherent oscillations present. B = 600 G, I_{arc} = 25A, V_{arc} = 35 V. Lower curve, no diffusion wave. Upper curve, diffusion wave at 4.0 cm from arc core shows applied 60 KHz plus increased amplitude in a range of frequencies on either side.

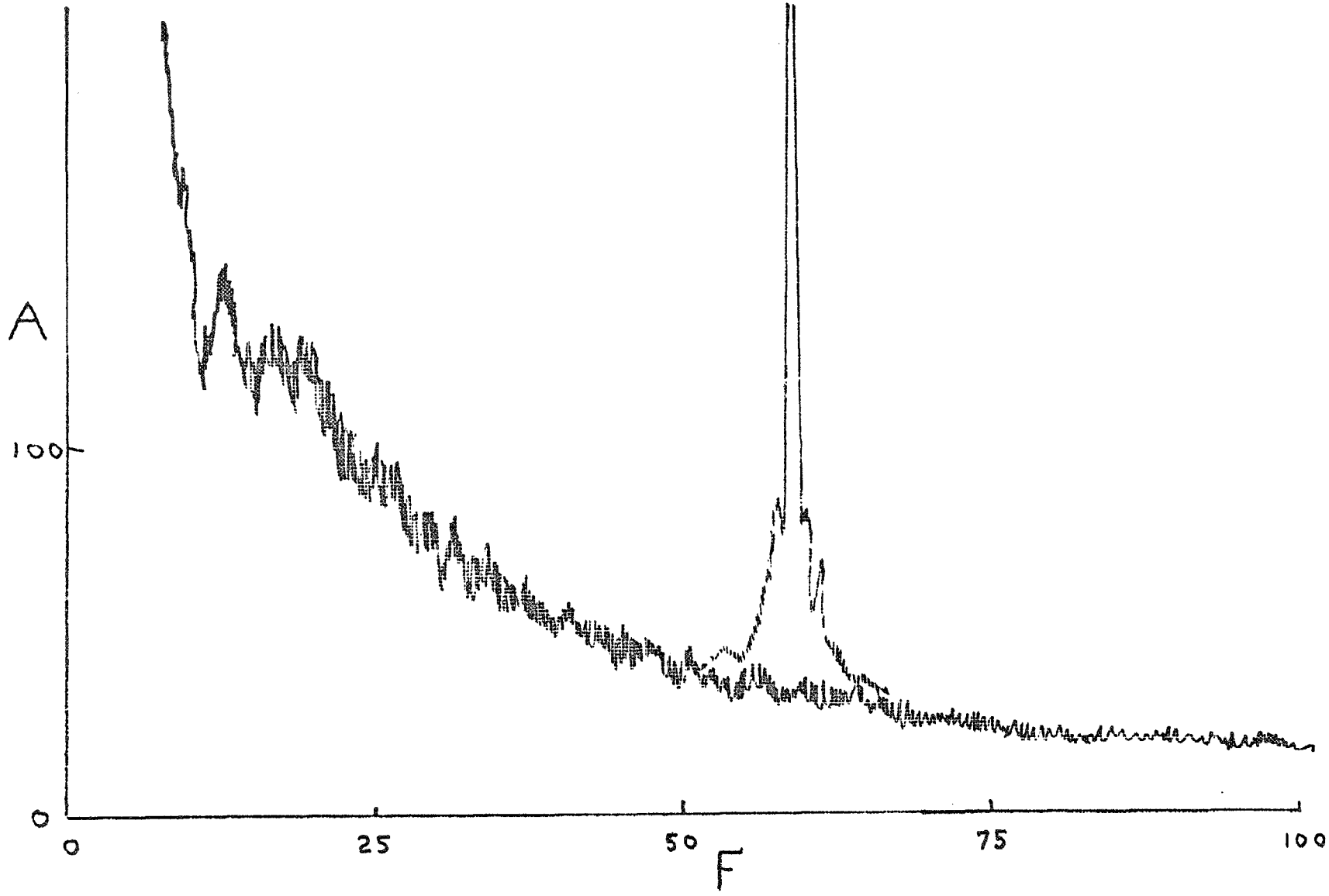

Fig. 9

8-21

Amplitude vs. Frequency, 0 - 100 KHz; No coherent oscillations present. B = 600 G, I_{arc} - 25A, V_{arc} = 35 V. Lower curve, no diffusion wave. Upper curve, diffusion wave at 4.5 cm from arc core showing applied 60 KHz and only very closely adjacent frequencies increased in amplitude.

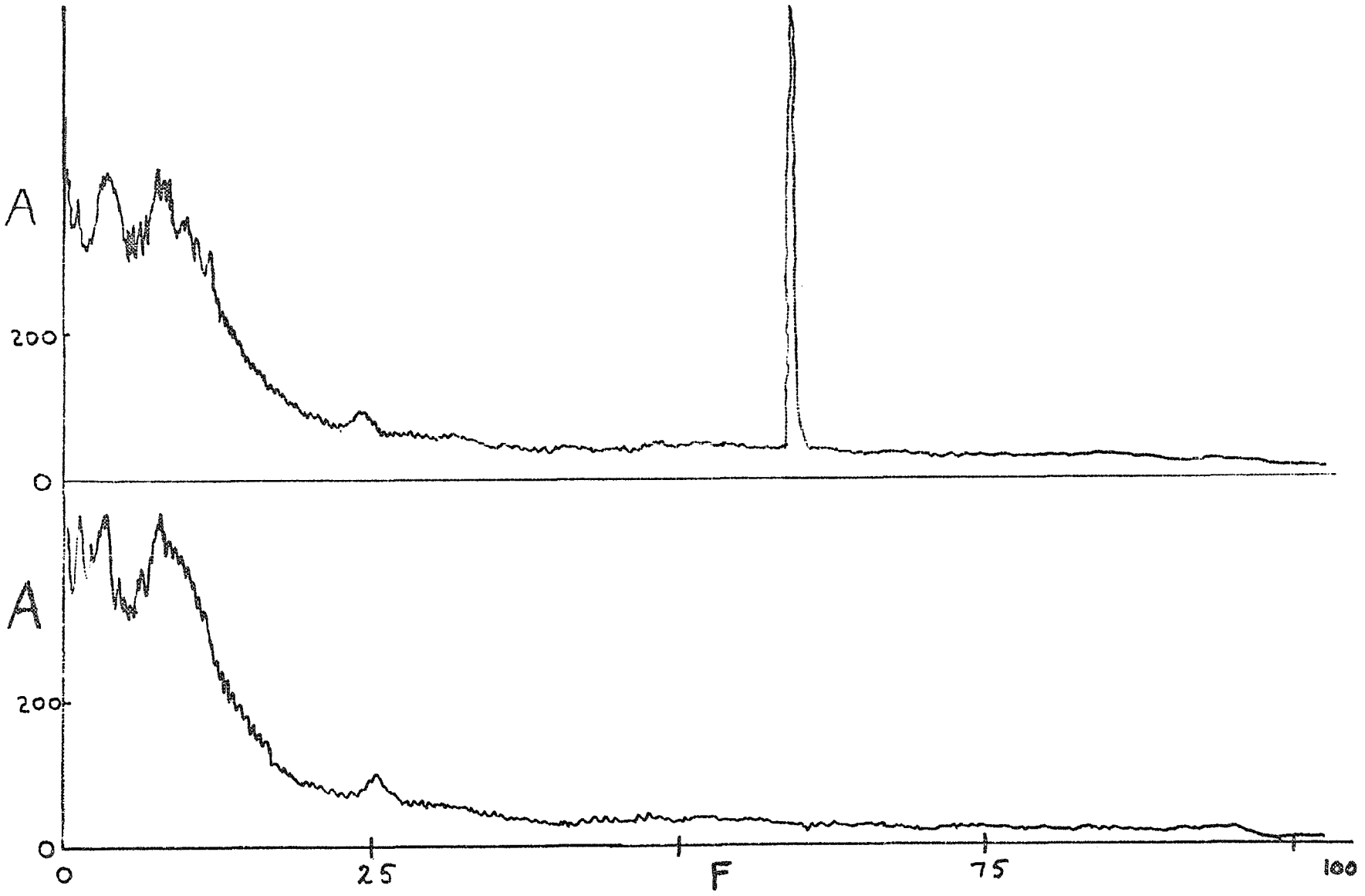

Amplitude vs. Frequency 0 - 100 KHz; Higher magnetic field than in Fig. 9. B = 1500 G, I_{arc} = 25A, V_{arc} =35 V. Lower curve, no diffusion wave. Upper curve, diffusion wave at 4.5 cm from arc core showing applied 60 KHz and no effect on the turbulent spectrum.

IV. Feedback Stabilization

A. Introduction

Much of the work carried out recently at Rensselaer is concerned with establishing whether anomalously high loss rates of charged particles from a plasma confined by a magnetic field are related to the presence of turbulence and coherent instabilities. In order to quantitatively investigate the physical mechanisms involved, it is necessary to be able to control the magnitude of these oscillations by means other than altering external parameters such as gas flow-rate, pressure and magnetic field. We have recently developed feedback stabilization techniques to apply to these previously identified instabilities in the Rensselaer HCD source[4]. The preliminary results presented in this report deal mainly with one of the coherent instabilities, the drift-dissipative wave. We find that the amplitude of this instability can be controlled over a range from complete suppression (to the noise level), to an enhancement factor of approximately two.

The stabilization system developed involves: (1) a sensing or monitoring element which provides a signal proportional to the magnitude of the instability, (2) a phase-shifting, amplifying network, and (3) a suppressing element by which a nulling or compensating signal is fed back into the plasma. The initial work reported here involved the use of Langmuir probes as both sensing and suppressing elements, but the major objective of the program is to develop remote sensing and suppressing, applicable to higher energy density plasmas where it is not feasible to introduce elements within the plasma confining chamber. Further, such a technique would produce the minimum perturbation of the plasma medium.

Work on stabilization techniques in a variety of plasma devices has been reported by many authors with varying degrees of success; for example Arsenin and Chuyanov[12], Keen[13,14,17], Parker and Thomassen[15], Simonen et al[28], and Tanaca and Hagi[29], have done experiments on the drift wave using localized feedback elements.

Variations of the type of suppressor element have been investigated by Chen[18,19], where neutral beams were employed, and Chu et al[20] used microwaves. Infrared lasers have been proposed[21] as the suppressing element, but no experimental work has been performed.

Extending this technique to other instabilities; Garscadden and Bletzinger[22] have used feedback to stabilize an ion acoustic wave, while work on the transverse Kelvin-Helmholtz instability has been reported by Carlyle[23], Chu et al[24], and Simonen[25]. Attempts to control the cyclotron instability have been made by Arsenin, Zhil'tsov, Likhtenshtein and Chulnov[26].

A part from the microwave experiment and those using neutral beams, all the suppressing elements used to date have commonly been large plate electrodes. These devices may perturb the plasma by their contact with it and thus are undesirable.

B. Feedback Stabilization System

The feedback stabilization system developed is shown in block diagram form in Fig. 12. The sensor probe was biased at -50 v (ion saturation region), and the current drawn was passed through a resistor to yield a voltage proportional to the charged particle density (current) fluctuations associated with the instability. This signal was then filtered by the selective amplifier, resulting in a 3 - 4 KHz bandwidth, centered at the frequency of the instability. The reason for attenuating the remainder of the frequency spectrum was to avoid the possibility of the suppressor signal containing frequencies which could excite higher order eigenmodes of the instability. The a.c. suppressor signal was then phase shifted, amplified and applied to the suppressor probe through a biasing network. The biasing network allows the suppressor electrode to be at either a positive or a negative d-c level with respect to the plasma.

Three probes were used, all of 20 mil diameter tungsten wire and 5 mm long. The probes are movable radially, and sensor and suppressor probes are separated axially by approximately 1 cm. The detecting probe is located 30 cm away from the feedback elements, at the same azimuthal position. It is biased exactly as the sensor probe. All quantitative measurements of the amplitude of the instability are read from the detector probe signal, using the wave analyzer as a frequency selective voltmeter.

Measurements are made of the amplitude of the instability, both in the unperturbed state (no feedback), and during the application of the suppressing signal. The gain of the feedback system, the phase shift introduced by the feedback network, and the change in frequency of the instability under the application of the suppressor signal are also recorded. The amplitudes, gain, and frequency can all be accurately measured by the model 310 wave analyzer. Phase shift is measured to within 5^{o} through the use of a PAR-HR-8, precision lock-in amplifier. This is a significant improvement over the error inherent in phase measurement systems used in other laboratories.[16] Gain and phase are measured at the suppressor probe, with the input to the phase shift network as the reference.

Although data acquisition would seem straightforward, several problems are introduced by the dynamics of the feedback network, the instrumentation and the turbulence of the arc discharge, reflected in the noise level of the signals involved.

The noise problem cannot be completely resolved and indeed the effect of these turbulent plasma fluctuations represent a major interest in this work. Efforts have been made to prevent any externally introduced noise level below that inherent in the arc itself, by using low noise components

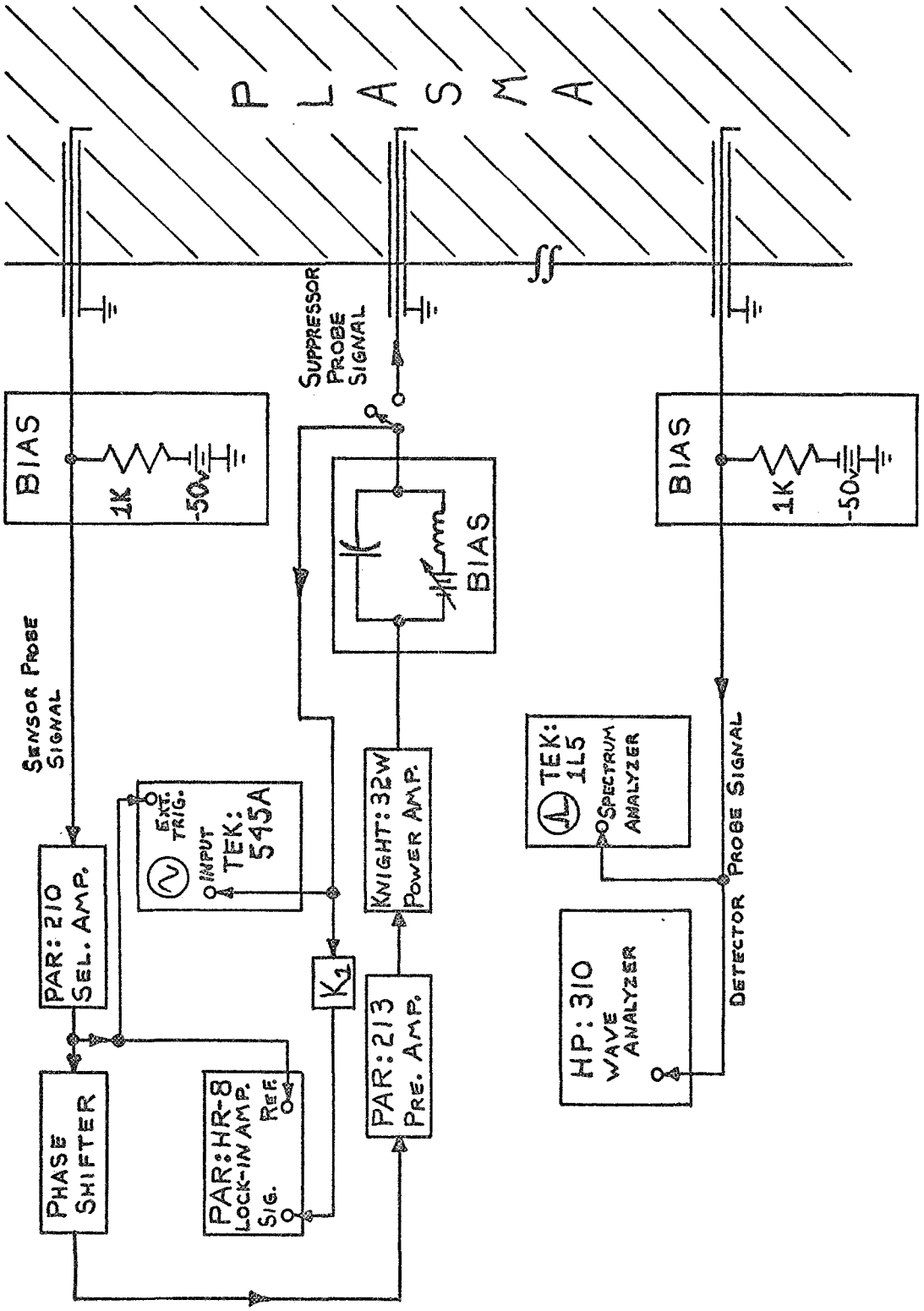

FIGURE 12 Feedback Stabilization System: Block Diagram

such as the 213 preamplifier. Noise can significantly degrade the reliability of any measurement, especially that of phase. Thus a simple phase measurement system, such as an externally triggered oscilloscope, is totallly inadequate for our purposes. The major reason for employing the HR-8 lock-in amplifier to measure phase is its ability to distinguish coherence even when there is only a small signal to noise ratio.

The problems in instrumentation have all been satisfactorily overcome except for that caused by the extreme non-linearity of the dynamic response of a Langmuir probe, and the fact that the probe response changes with position in the arc. In essence we have an impedance matching problem where the input resistance changes by four orders of magnitude over the dynamic range involved. This problem cannot be entirely solved since it is inherent in the device. It has been found, however, that best results are obtained by biasing the suppressor probe slightly positive with respect to floating potential (electron collecting).

There is one other problem introduced by the dynamics of the system that makes necessary particular care in measurement. As will be shown in the next section, the instability frequency changes as a function of phase shift. This presents an instrumentation problem in the measurement of the phase shift introduced. It is necessary to continually monitor this frequency change, otherwise significant phase errors, of the order of 40° can result, since the HR-8 utilizes high Q, tuned amplifiers. This source of error can be eliminated by retuning the reference channel of the HR-8 for each measurement. This is a valid procedure as the Q of the reference channel is the same as the Q of the signal channel, both being set by external controls.

After elimination or reduction of the instrumentation problems outlined above, the system developed has provided data with a high degree of reproducibility. Furthermore, the basic components of the system are readily adaptable to the use of other types of sensor and suppressor elements.

C. Feedback Stabilization of the Drift Wave

1. Theoretical Considerations

The feedback stabilization system was developed for the purpose of studying plasma turbulence in the presence of controlled amplitude, coherent oscillations. No satisfactory theory applicable to our inhomogeneous, highly ionized plasma has been devised to explain how stabilization works. Keen[13] has used a phenomenological approach to a theory, based on his experiments in a somewhat similar device. He makes use of the Van der Pol equation[27], modified to include a phase shift term, $n_1(\tau)$: [$\tau = t - T$; T = the delay time; $\omega T = \phi$, the phase shift = constant.]

$$\frac{d^2 n_1}{dt^2} - (\alpha - \beta n_1^2)\frac{dn_1}{dt} + \omega_0^2 n_1 + g\omega_0^2 n_1(\tau) = 0 \qquad (4\text{-}1)$$

n_1 = density fluctuation

ω_o = natural frequency of the oscillation

α = linear growth rate of the oscillation

β = non-linear saturation coefficient of the oscillation

g = absolute gain of the feedback system

τ = quasi-time

The modification to Van der Pol's equation, $g\,\omega_o^2\,n_1(\tau)$, represents the density fluctuation phase-shifted, (τ); and amplified, (g).

Writing equation (1) in the form of a difference-differential equation and assuming a solution of the form $n_1 = a \sin \omega t$, the following conditions hold for the steady state:

$$a_o^2 - a^2 = -g\,(\omega_o^2/\alpha\omega)\,a_o^2 \sin \phi \tag{4-2}$$

$$\omega^2 = \omega_o^2\,(1 + g \cos \phi) \tag{4-3}$$

where $a_o = (4\alpha/3\beta)^{1/2}$ = unperturbed amplitude

and a = perturbed amplitude

Rearranging equation (2):

$$(a/a_o)^2 = 1 + g\,\left(\frac{\omega_o^2}{\alpha\omega}\right) \sin \phi \tag{4-4}$$

Effect of Phase:

This predicts that $(a/a_o)^2$ will vary as $\sin \phi$ when the phase shift is changed, with greater variation for higher values of gain, and optimum suppression at 270°. ($\sin 270^\circ = -1$). Equation (3) predicts $\omega = \omega_o$ at $\phi = 270^\circ$; therefore, with ϕ for optimum suppression, we have:

$$(a/a_o)^2 = 1 - g\,\left(\frac{\omega_o}{\alpha}\right) \tag{4-5}$$

Effect of Gain:

This predicts a linear decrease of $(a/a_o)^2$ from 1 to 0 as g is increased from 0 to α/ω_o.

Returning to equation (3), taking the square root of each side we obtain:

$$\omega = \omega_o\,(1 + g \cos \phi)^{1/2} \tag{4-6}$$

At maximum suppression $g_{max} = \alpha/\omega_o < 1$, therefore $(g \cos \phi)^2 \ll 1$ and (6) can be expanded to yield:

$$\omega = \omega_o \left[1 + \frac{g \cos \phi}{2} - \frac{(g \cos)^2}{8} + - \ldots\right]$$

$$\omega \approx \omega_o \left[1 + \frac{g \cos \phi}{2}\right]$$

$$\omega - \omega_o = \Delta\omega = \frac{\omega_o}{2} g \cos \phi \qquad (4\text{-}7)$$

$$\frac{2\Delta\omega}{\omega_o} = g \cos \phi$$

Equation (7) predicts the frequency of the instability will change with phase shift and follow a cosine variation. It also predicts larger frequency changes for higher gains.

Realizing the limited validity of the model represented in the Van der Pol approach, it is expected that this theory will only indicate the major trends to be expected in any real feedback system. This is confirmed by the experimental data presented in the next section.

2. Experimental Results

Presented in this section are preliminary results exhibiting the ability of the feedback system to control the amplitude of the drift instability which develops in the plasma under certain operating conditions of the arc.

Equation (5) of the preceeding section predicts a linear plot of $(a/a_o)^2$ *vs.* Gain, with ϕ set for optimum suppression. This data is shown in Fig. 13 for several radial separations of the sensor and suppressor probe. It can be seen that $(a/a_o)^2$ is a monotonically decreasing function of the gain, although the relationship is not linear as predicted by (5), except over a small range of gain. Fig. 13 shows also that best results are obtained when the suppressor probe is located in the region where the instability has its maximum growth rate; and that as the radial separation is increased, suppression becomes less effective.

Data of $(a/a_o)^2$ *vs.* phase shift, for two different gains, is presented in Fig. 14. It is readily apparent that greater suppression occurs at higher gain, as predicted by equation (4). This equation also predicts a functional variation of sin ϕ for $(a/a_o)^2$, where ϕ is the phase shift. The data is in agreement with this predicted variation, but optimum suppression occurs at approximately 300^o instead of 270^o.

Fig. 15 shows the change of frequency of the instability as a function of phase shift. Equation (7) predicts a cos ϕ variation. The data definitely shows this trend.

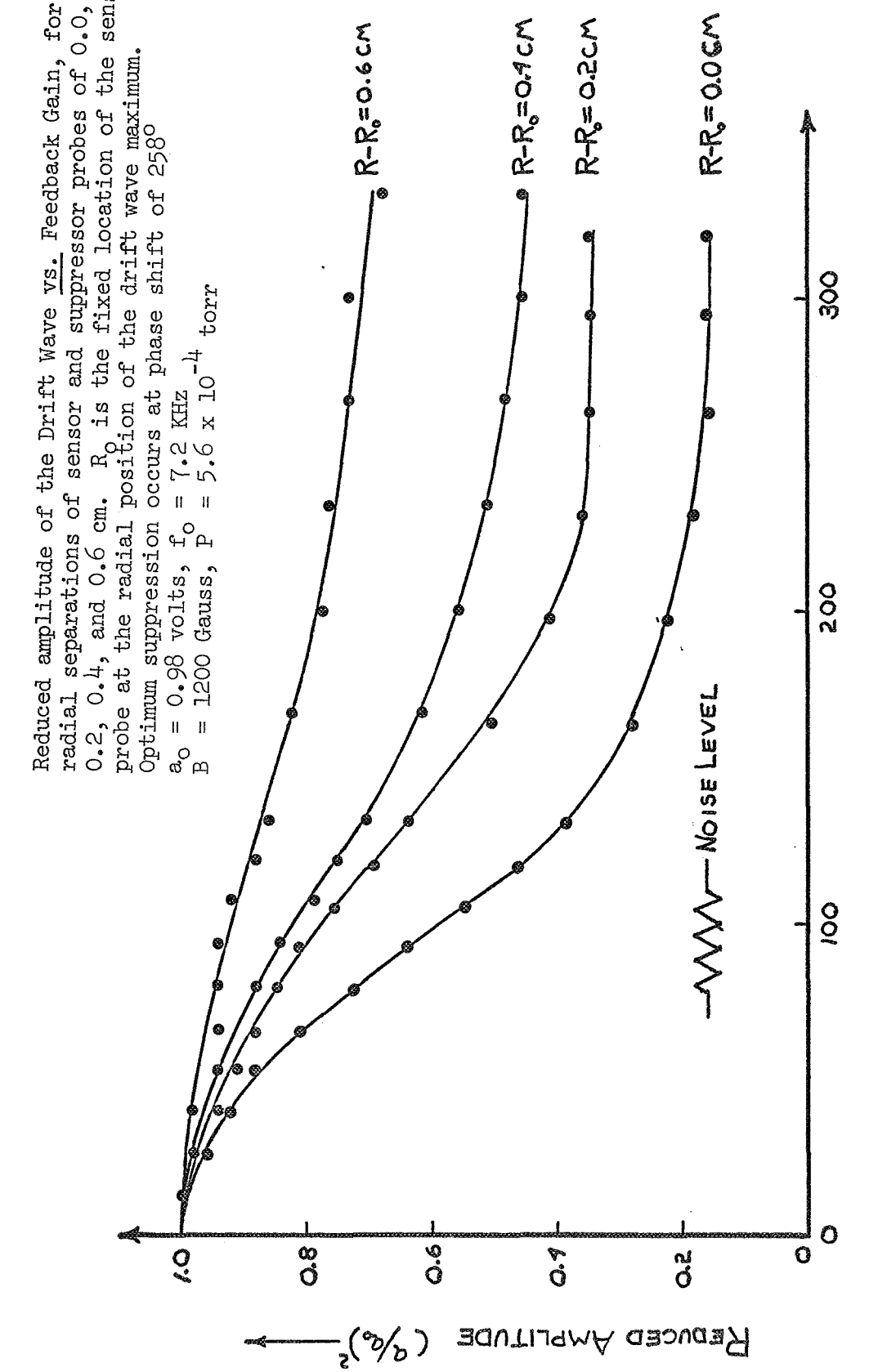
Reduced amplitude of the Drift Wave vs. Feedback Gain, for radial separations of sensor and suppressor probes of 0.0, 0.2, 0.4, and 0.6 cm. R_o is the fixed location of the sensor probe at the radial position of the drift wave maximum. Optimum suppression occurs at phase shift of 258°
a_o = 0.98 volts, f_o = 7.2 KHz
B = 1200 Gauss, P = 5.6 x 10^{-4} torr
R-R$_o$=0.6 CM
R-R$_o$=0.4 CM
R-R$_o$=0.2 CM
R-R$_o$=0.0 CM
NOISE LEVEL
REDUCED AMPLITUDE $(a/a_o)^2$
1.0
0.8
0.6
0.1
0.2
0
100
200
300
FEEDBACK GAIN

FIGURE 13

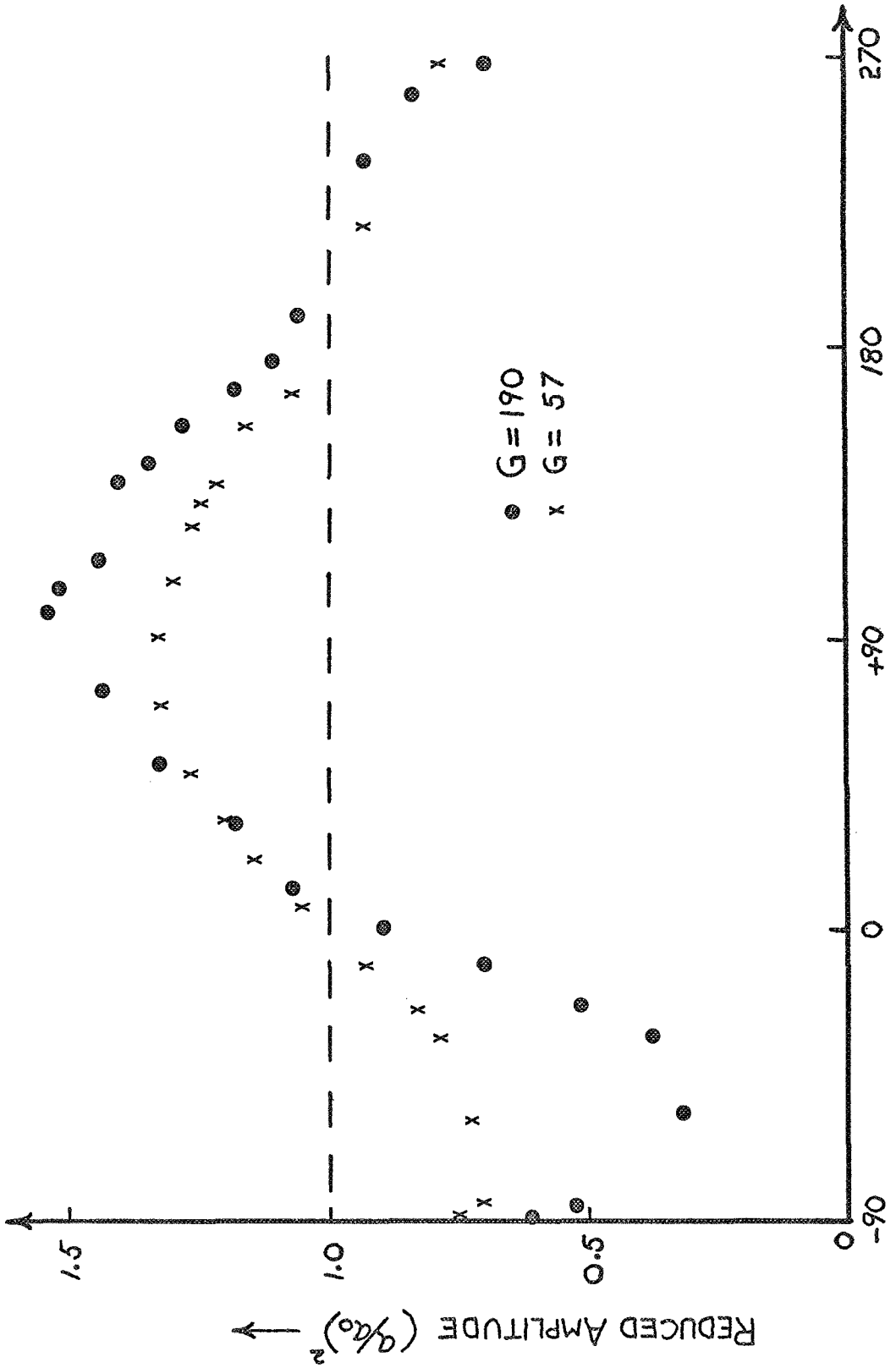

Fig 14

Reduced amplitude of the drift wave vs. phase shift, for two different gains (190 and 57). Sensor and suppressor probes at R = 1 cm = drift wave maximum.
a_o = 1.0 volts, f_o = 6.8 KHz
B_o = 1335 Gauss, P = 5.0 x 10^{-4} torr

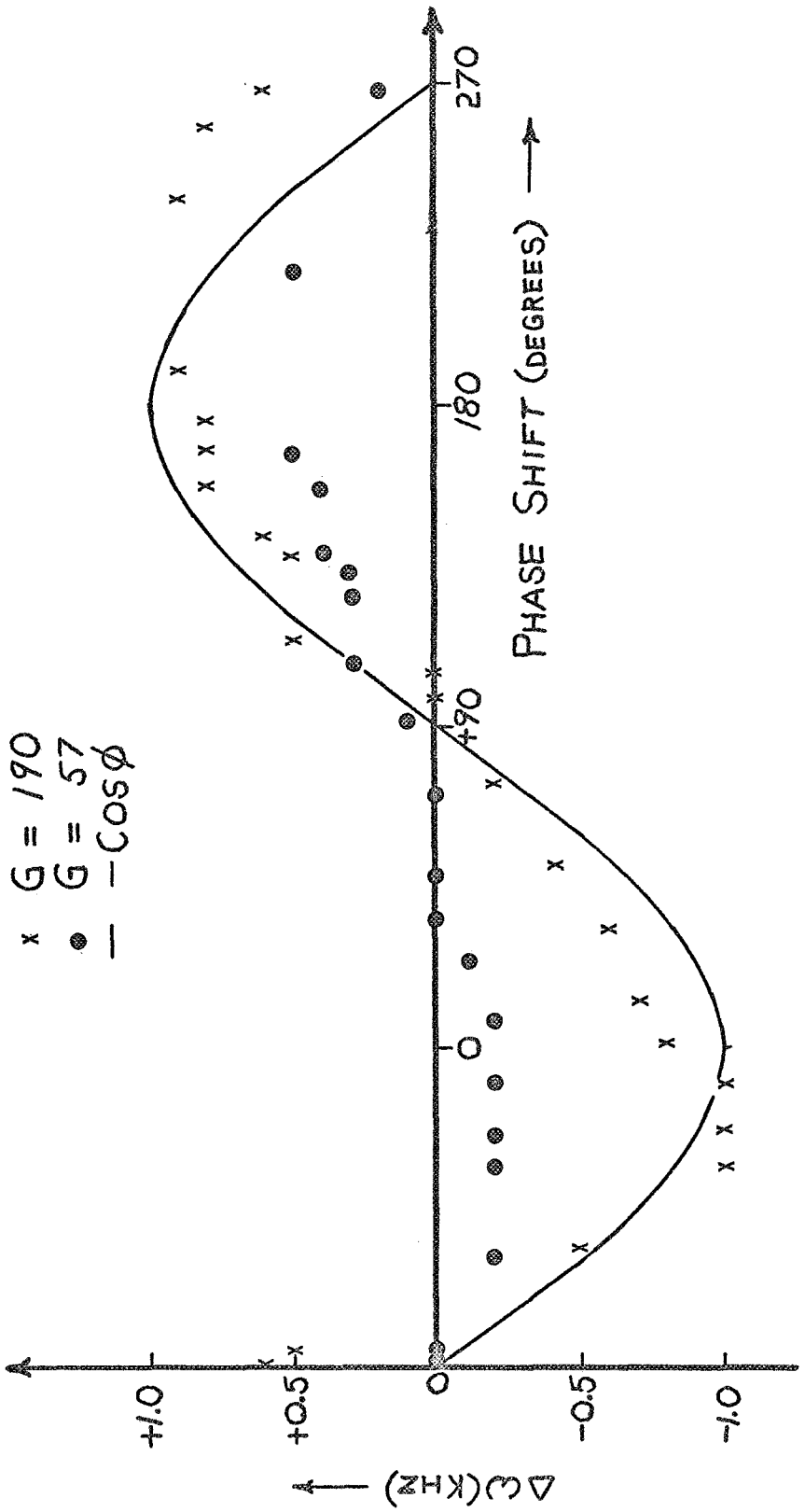

Fig. 15 Frequency change of the drift wave vs. phase shift under the conditions as for Figure 14. For comparison purposes, the solid line is a plot of cos ϕ.

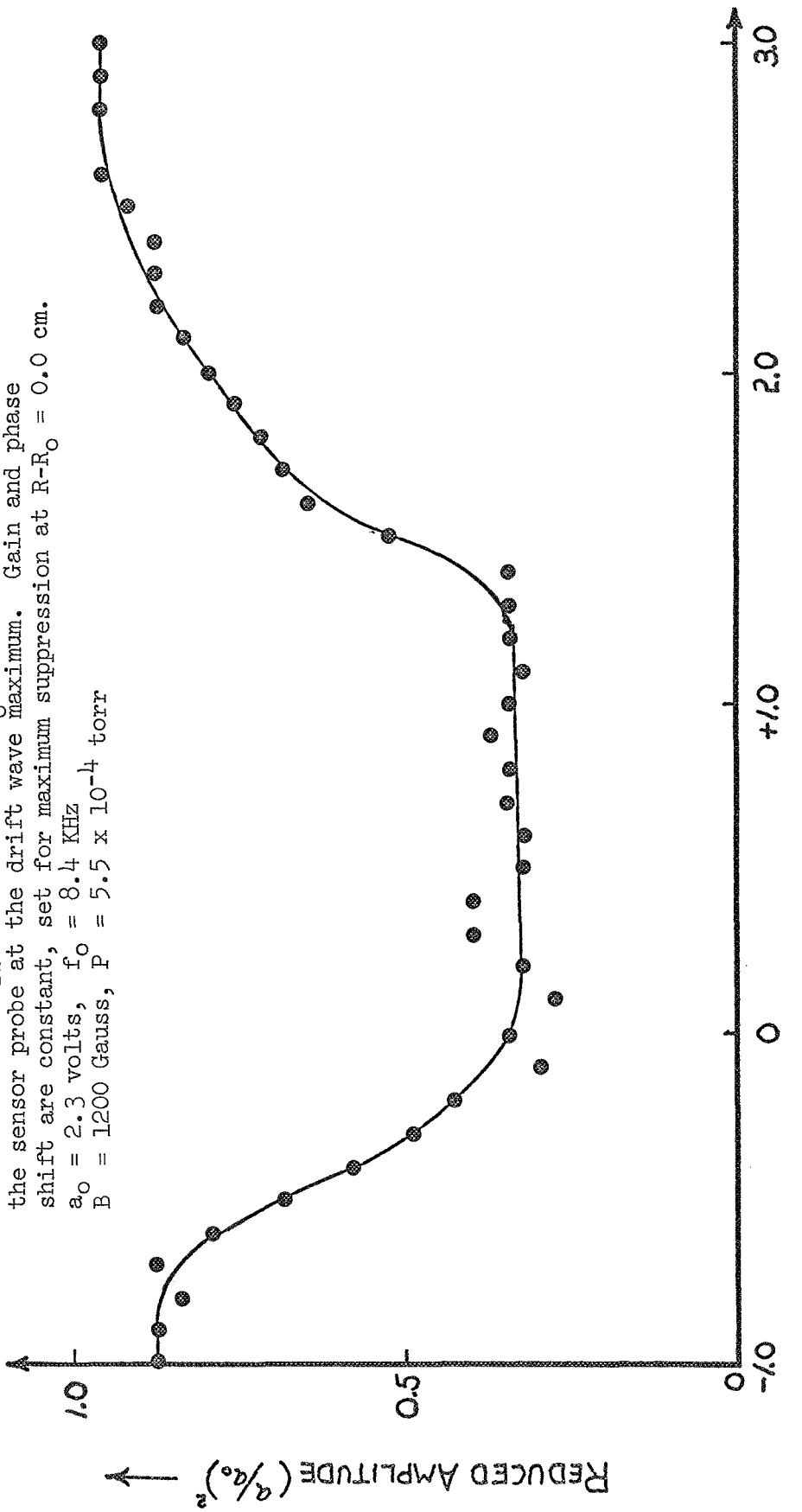
Reduced amplitude of the drift wave vs. the radial separation of sensor and suppressor probes. R_o is the fixed location of the sensor probe at the drift wave maximum. Gain and phase shift are constant, set for maximum suppression at $R-R_o$ = 0.0 cm.
a_o = 2.3 volts, f_o = 8.4 KHz
B = 1200 Gauss, P = 5.5×10^{-4} torr
REDUCED AMPLITUDE $(a/a_o)^2$ ⟶
1.0
0.5
0
-1.0
+1.0
2.0
3.0
R - R_o (cm) ⟶

FIGURE 16

Represented in Fig. 16 is $(a/a_o)^2$ vs. $R-R_o$, the radial separation of the sensor and suppressor probes. The sensor probe is fixed at the drift wave maximum, R_o; and the phase shift and gain are kept constant at their values for maximum suppression at $R-R_o = 0$ cm. This graph points out the effect of the spatial separation, and allows an estimate of the spatial coherence length of the instability. The suppressor signal should be injected within a spatial coherence length of the sensor signal in order to achieve suppression. The magnitude of the spatial coherence length is of order 1.5 cm for the conditions under which the data shown in Fig. 16 was taken.

Fig. 17 is included in this discussion for completeness and shows the variation in amplitude of the drift wave as a function of $R-R_o$, without feedback. Under these particular operating conditions R_o was 1.0 cm from the core of the plasma. The radial location at which maximum amplitude of the drift wave occurs changes, (lying closer to the arc core), as the external magnetic field is increased.

3. Discussion

Keen's[13] data fitted the equations presented earlier remarkably well. His highly ionized plasma was somewhat similar to ours, but there were several differences in apparatus and technique.

The biggest difference in the feedback system was that Keen used up to four large plate electrodes for his suppressing elements. These are in contact with the outer region of the plasma and the presence of the suppressor elements alone may significantly perturb the plasma. A Langmuir probe is a much more localized element.

Keen used up to four separate feedback loops for suppression, whereas we employed only one.

These two differences could account for any variations in observed results. Moreover his device is not exactly like our HCD. Keen's hollow cathode arc has baffles and differential pumping, with an electrostatic field-free region for the plasma, and a lower level of plasma turbulence than we observe. Such a regime of operation could also be achieved in our device, but would defeat the purpose of studying the effects of turbulence on plasma properties.

The phenomenological approach through Van der Pol's equation can be used to explain the observed experimental observations. However a theory, derived from basic plasma equations, relating the constants and variables of this equation to parameters of the discharge would be much more desirable for a fuller understanding of feedback stabilization. Simonen, Chu, and Hendel[28] have used this approach successfully on their Q-machine. The difference between thermal cesium plasmas and HCD plasmas precludes any attempt to apply this theory directly to our device. A modified form relating

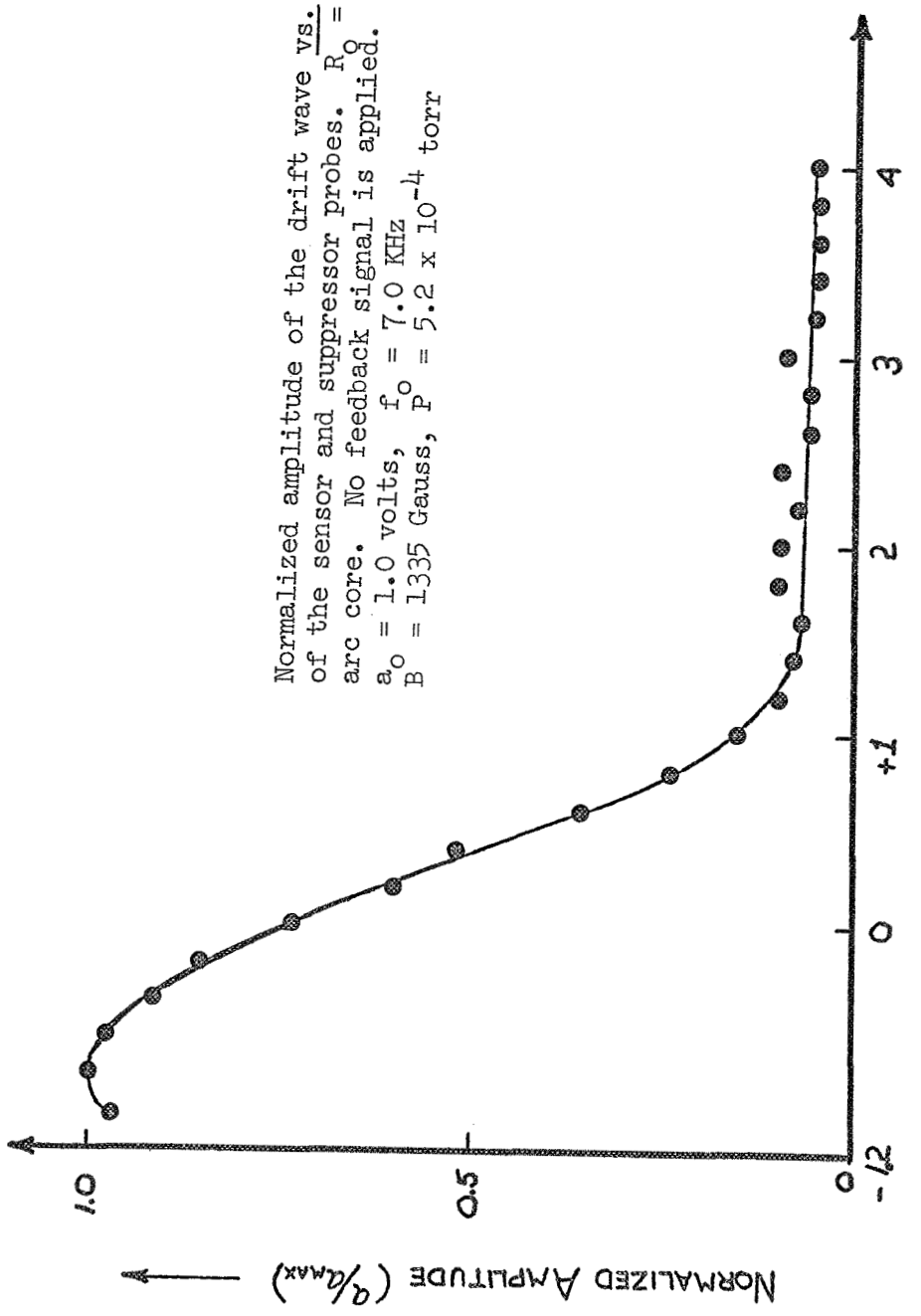
Normalized amplitude of the drift wave vs. radial separation of the sensor and suppressor probes. R_o = 1.0 cm from the arc core. No feedback signal is applied.
a_o = 1.0 volts, f_o = 7.0 KHz
B_o = 1335 Gauss, P_o = 5.2 x 10^{-4} torr
NORMALIZED AMPLITUDE (a/a_{max}) ⟶
1.0
0.5
0
-.2
0
+1
2
3
4
R-R₀ (cm) ⟶

FIGURE 17

density, temperature, their spatial gradients, collision times, electric fields, etc. may well be successful. For example, the 'apparent' discrepancy in the predicted value of the phase shift for maximum suppression may be related to the phase difference between the charged particle density and potential fluctuations associated with the drift wave.

V. Optical Detection Techniques for Plasma Instabilities

A. Introduction

An optical technique has been developed for detecting and measuring plasma instabilities in the Rensselaer hollow cathode discharge by monitoring fluctuations in the intensity of the light emitted by the plasma. The initial interest in this system arose from investigation of feedback stabilization of plasma instabilities which is described elsewhere in this report. The feedback loop requires a remote sensing element capable of detecting the instability without perturbing the plasma.

Although Langmuir probes are the simplest and best understood diagnostic elements, their usefulness in a feedback stabilization system is limited by the fact that their performance may be rapidly degraded when used in high energy plasma devices. An optical system, on the other hand, offers two major advantages over the Langmuir probe. First, by monitoring spontaneous light emission, an optical measurement in no way disturbs the plasma medium under consideration. Secondly, an optical system allows measurements to be made in any region of the plasma, regardless of temperature if a reasonable degree of optical thinness exists. An optical system usually, however, has one distinct disadvantage when compared to a Langmuir probe. An optical system lacks a high degree of spatial resolution and yields information which is averaged over a much large volume of the plasma than obtained by a Langmuir probe. The system we have developed, however, demonstrates good spatial resolution perpendicular to its optical axis, and some resolution along its optical axis. The system has not only shown itself to be a sensor of a fully developed instability, but has proven to be a useful diagnostic tool; for example, it has allowed exploration of the core of the hollow cathode discharge where Langmuir probe measurements cannot readily be made.

B. Design and Operation

The optical sensor consists of a 14 inch single-stage boresight optical system built to fit an existing probe port on the Rensselaer hollow cathode discharge. The boresight consists of three lenses: a 30 mm focal length microscope objective, a 125 mm eyepiece, and a 34 mm field lens mounted on movable stops in a cylindrical housing fitted inside the Pyrex probe port. The boresight actually acts as a periscope by guiding light from the plasma through the long, narrow arm of the probe port and forming a three dimensional image of the plasma core and the surrounding lower density plasma at a location 44 cm from the end of the Pyrex arm. A sampling slit of adjustable width, which can be moved either along the optical axis or transverse to it, is positioned within the three dimensional image. Positioning of the sampling slit allows light from a certain spatial region of the plasma to pass through it, while blocking light from other regions. This allows greater spatial resolution than most optical systems, where the aim is to focus as much light as possible on a single focal plane. The Rensselaer system strives to separate the planes of optimum focus, reducing the

depth of focus by using low f numbers. Data taken with slits of different size oriented in a direction transverse to the optical axis and located at different positions along the optical axis of the lens system indicate that the longitudinal resolution is about an order of magnitude below that in the transverse direction; thus we could examine light from a region of the plasma defined by the cross-sectional area and position of the slit so that we sample a region 1 mm long transverse to the axis but 1 cm in extent along the optical axis. Measurements of relative modulation of light intensity, as discussed later, are in agreement with approximate calculations of the depth of focus and degree of resolution to be expected from the optical system.

Light passing through the sampling slit is reimaged, using another lens, on the entrance slit of a 1/4 m Ebert type grating monochromator. Light output from the monochromator is detected by an R 212 photomultiplier tube and the signal voltage is measured across the photomultiplier load resistor. The total signal voltage is taken as a measure of the overall light intensity at the optical wavelength selected by the monochromator and is measured directly on an integrating digital voltmeter.

Along with the position of the sampling slit, the other variable parameter of the system is the wavelength setting of the monochromator. Suitable adjustment allows selection of individual argon lines, or a section of the continuum spectrum. Further adjustment allows recording of wideband light signals consisting of light of all wavelengths falling on the entrance slit.

The time-dependent part of the photomultiplier signal represents time-dependent fluctuations in the light intensity falling on the photomultiplier. These intensity fluctuations are related to fluctuations of the plasma corresponding to the instability. The photomultiplier signal is amplified by a PAR 213 Preamplifier before being displayed on a Tektronics Spectrum Analyzer, and processed by a H.P. 310 Wave Analyzer. Fig. 18 shows the system in block diagram.

Data is taken by recording the frequency spectrum output of the wave analyzer on an X-Y Recorder, measuring the instability peak amplitude and the noise level and recording the digital voltmeter reading. A relative modulation factor is computed by normalizing each signal value to the respective overall light intensity measured by the DVM, i.e.

$$\text{Relative Modulation} = (V_{peak} - V_{noise})/V_{DVM}.$$

Previously, instability data from the arc plasma has been presented in terms of peak amplitude alone. In some optical measurements, however, the noise level can be appreciable compared to the peak signal level (see Fig. 20 and Fig. 19). Further, since the overall light intensity changes rapidly over a small (radial) region of the plasma (see Fig. 22), it is necessary to normalize each measurement of a fluctuation in light intensity in terms of the overall intensity sampled by the instrument. Hence, what is measured is the fractional modulation of the optical signal at the frequency of the instability.

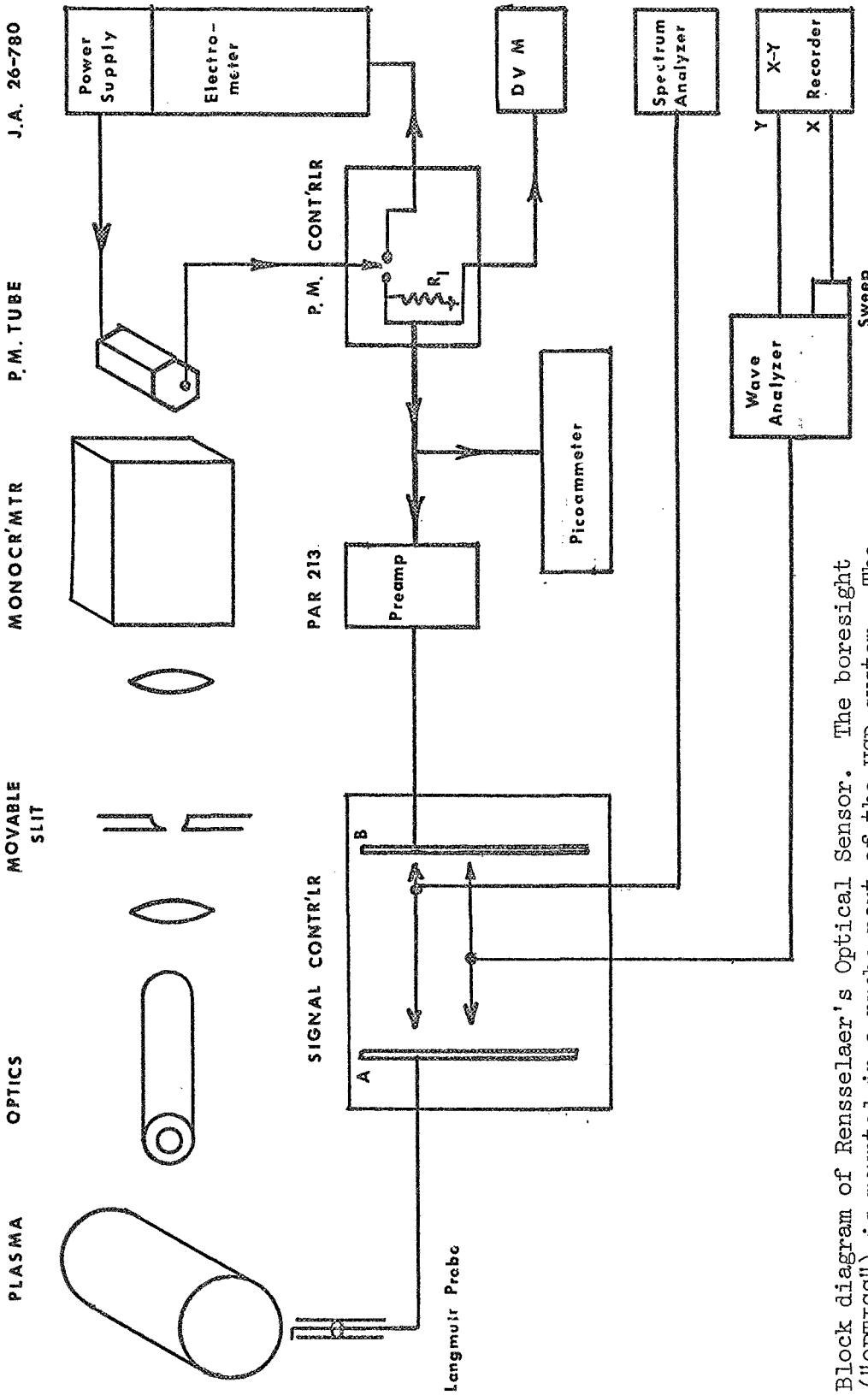

Fig 18

Block diagram of Rensselaer's Optical Sensor. The boresight ("OPTICS") is mounted in a probe port of the HCD system. The two lenses shown are external to the discharge device as is the movable slit. Langmuir probes are used for comparison. Data is taken from the DVM and XY Recorder

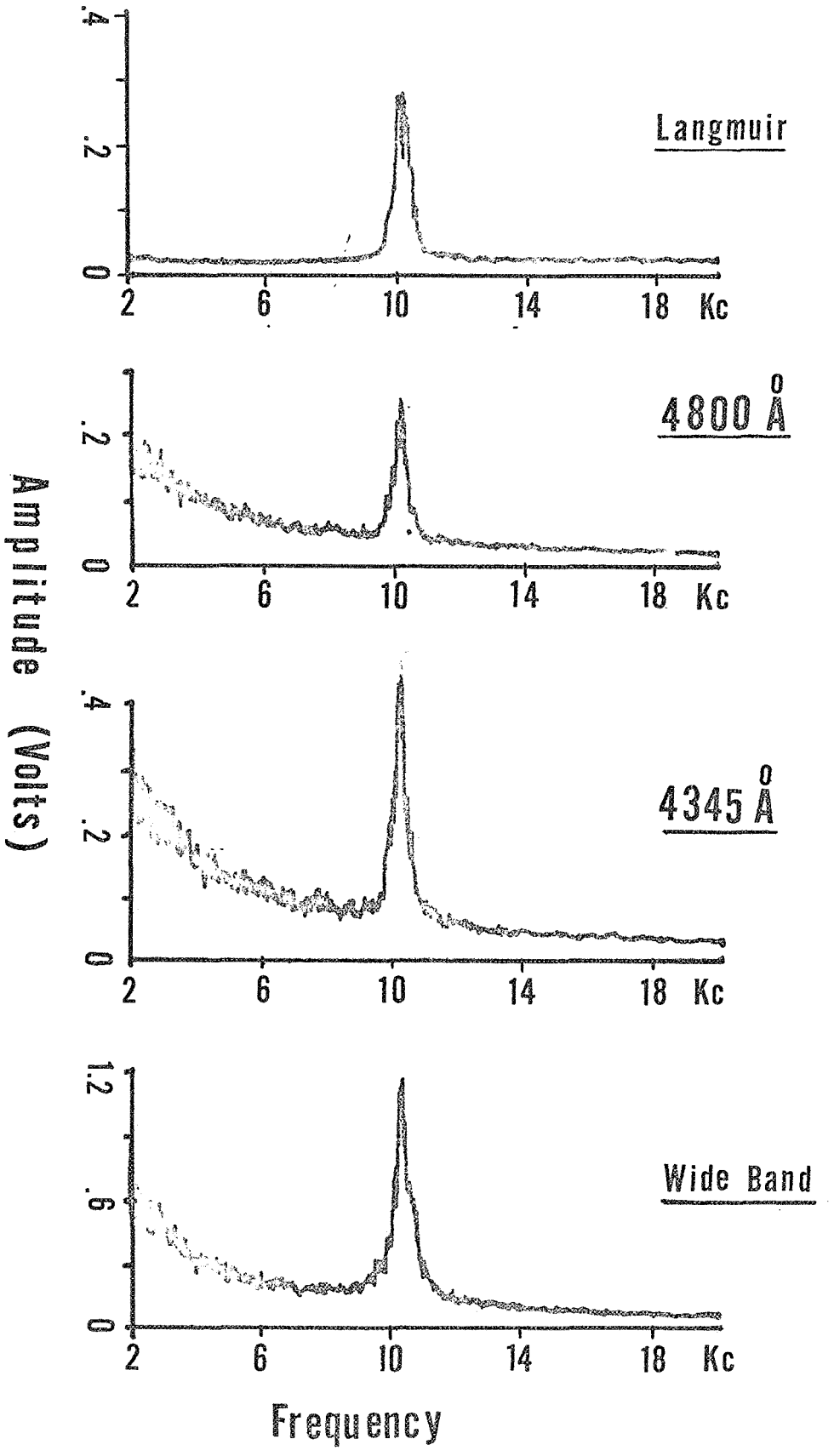

Frequency spectra of the drift wave instabilities at the edge of the core for Langmuir probe, Two Argon I lines, and a wide band sensor. Discharge condition: V_{arc} = 42 volts, I_{arc} = 20 Amps, Cathode flow = 6.0, Anode flow = 2.5, B = 2000 gauss

Fig 19

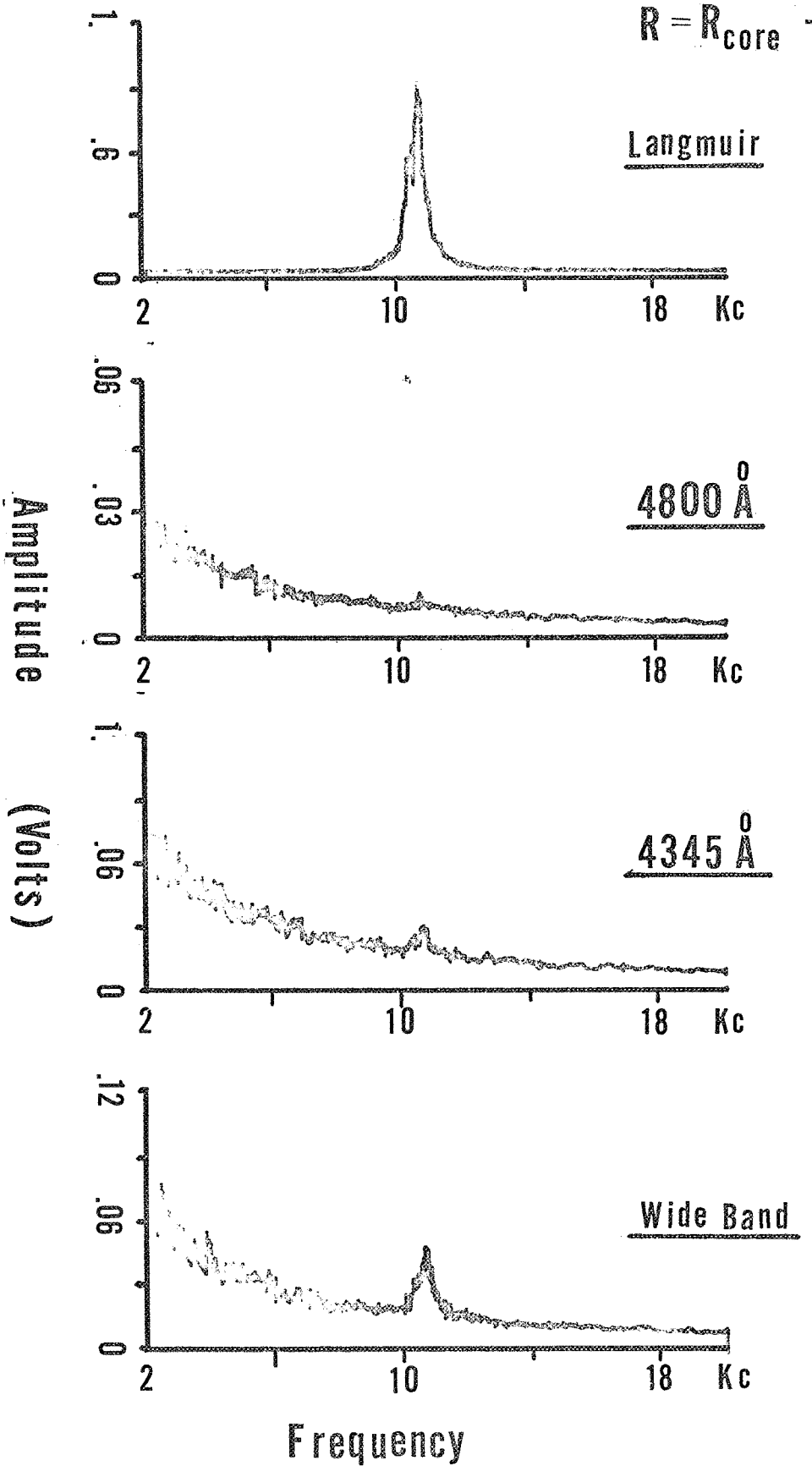

Frequency spectra under the same condition as Figure 19 taken at 0.5 cm from the edge of the core

Fig 20

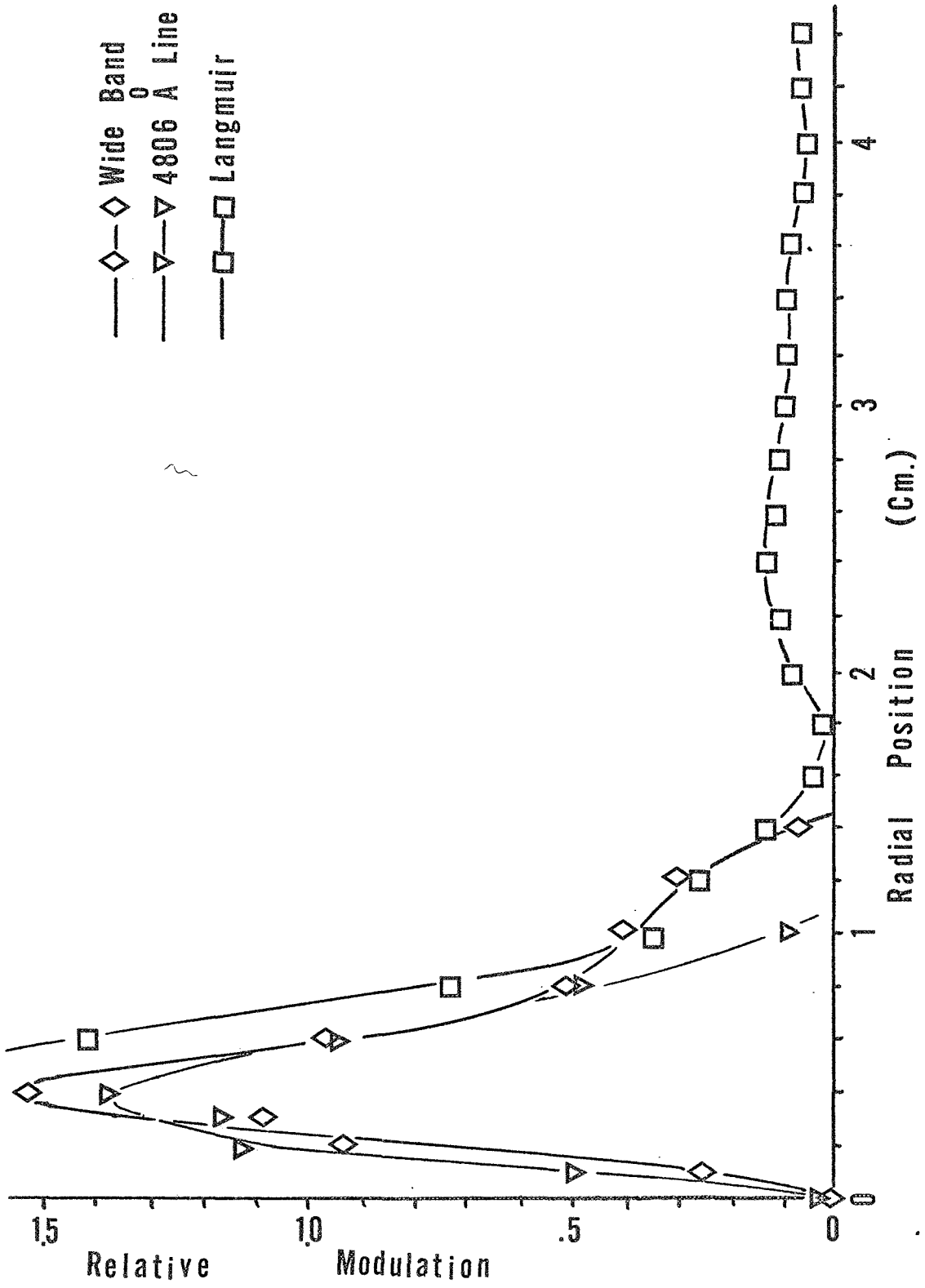

Fig 21

Comparison of radial profiles found from three different sensing techniques: Langmuir probe, single line and wide band optical sensors. Discharge conditions are the same as in Figure 19

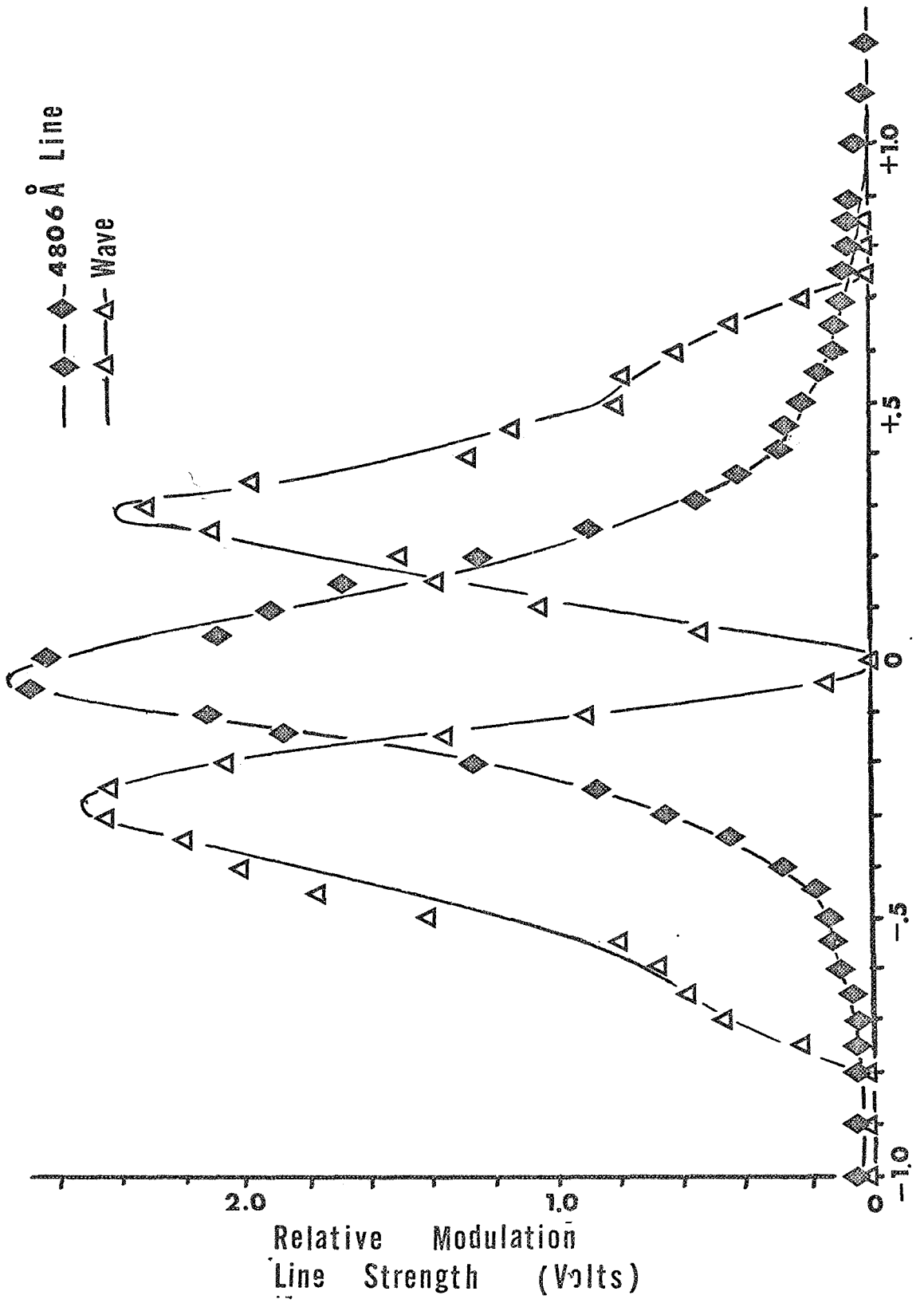

Fig 22

Radial Profile of the 4806 Å line showing cylindrical symmetry about the core. The figure shows the overall line intensity and the degree of modulation associated with the drift wave. Discharge conditions are the same as in Figure 19

Langmuir probe data, presented for comparison, is measured using the same instrumentation (Fig. 18) and is plotted using the same normalization procedure. For this case, the data represent the fractional modulation of the plasma potential.

C. Characteristics of the Optical Sensor

Examples of the frequency spectra obtained from the optical system are shown in Fig. 20 and Fig. 19. The figures show a comparison of the results obtained for the drift wave instability using a floating Langmuir probe, using two different Argon I lines and using the wideband configuration for two transverse positions of the sampling slit.

At the edge of the core (Fig. 19), where the Langmuir probe has reached the limit of its penetration without excessive heating, the two single line signals and the wide band signal behave similarly. All three show a large low frequency noise component with the ratio of the peak signal amplitude to the continuum signal level ("signal to noise ratio") ranging from 6 to 1 for the wide band signal to 7 to 1 for the 4345Å line. The Langmuir probe at the same position shows a signal to noise ratio of 9 to 1 which represents little improvement over the optical measurement.

Although data is shown for only two Argon I lines, the visible spectrum in the range of optical wavelengths from 3500 to 6000 Å has been compared for different transverse positions of the slit by sweeping the monochromator wavelength and recording the relative output of the photomultiplier. Results showed little or no change in the relative magnitude of the strongest Argon I, II and III lines. Relative modulation was compared for the 10 strongest lines at two slit positions and showed only small random variations from line to line with no particularly strongly modulated lines, or any discernable trends.

In general, the Langmuir probe gives better signal to noise ratios, especially far from the core. However, the optical system permits exploration of the core which has been impossible with a Langmuir probe. The wideband configuration demonstrates greater sensitivity at lower light levels than do single line measurements. This is illustrated in Fig. 3 where, at a distance of 0.5 cm from the edge of the core, the appearance of the Langmuir probe signal to noise ratio increases to 15 to 1, whereas the signals from both single line measurements are virtually lost in the noise. The large low frequency component remains, but the overall signal level is reduced. The wide band signal still shows the instability, but at a much reduced signal to noise ratio of approximately 2 to 1.

D. Radial Profile of the Drift Wave

The design of the optical sensor includes provisions for moving the sampling slit either transverse to or parallel to the optical axis. Figures 22 and 21 show the results of moving the slit in the transverse direction when the discharge conditions are adjusted to give rise to a strong drift wave.

Figure 21 shows a comparison of radial plots obtained from the Langmuir probe, the 4806 Å line and from the wide band sensor. In the core, for radii less than 0.5 cm, only the optical sensor can be used. The observed signal amplitude falls to zero with the slit adjusted to sample light from the central region of the core. For the discharge conditions used, the Langmuir probe and optical sensor give similar results from the edge of the core out to 1.6 cm, showing the amplitude of the drift wave falling to zero at roughly the same point. Beyond 1.6 cm where the overall light intensity collected by the boresight optics is very low, neither the 4806 Å line nor the wideband sensors yield any useful information. The Langmuir probe, however, continues to indicate the presence of the drift waves at reduced amplitude.

Figure 22 shows that although the overall light intensity increases when approaching the center of the core, the relative modulation representing the drift wave falls to zero. Because the noise level increases considerably in the core, frequency spectrum data alone does not rule out the existence of the wave in the core. Therefore the optical signal was also processed by a PAR 100 Signal Correlator. The auto correlation[30] measurements indicated no coherent oscillation in the center of the core.

This is the first time we have been able to use a technique for detecting the drift wave in the core itself. It is to be expected that the maximum amplitude of the driftwave would occur in the region of steepest gradients of either the density or temperature of the charged particle components of the plasma. Langmuir probe data show that a wave maximum occurs in the region of a steep ion density gradient just outside the core. The optical probe data of Fig. 22 give fresh information, but its interpretation is not straightforward. The data indicate that the relative modulation is zero at the center of the core. If the longitudinal resolution of the optical system is indeed allowing us to examine only the center of the core, and if problems of optical opacity and light intensity are not confusing the issue, then we have an interesting result. Further work is in progress to settle this matter.

It is also clear that the maximum amplitude of the driftwave does not occur in the region where a maximum occurs in the radial gradient of the 4806 Å light intensity. However this light intensity is connected with the neutral particle density rather than the charged particle density. The wave amplitude should correlate more strongly with the ion density. Clearly the use of the optical probe offers the opportunity of gaining a great deal more information in a region previously inaccessible for diagnostic purposes.

E. Future Investigation

In the future, it is planned to use the optical sensor to study the ion acoustic wave instability in a manner similar to that described for the drift wave. Preliminary work has shown that ion acoustic waves can also be detected with the optical sensor. It is also planned to evaluate, quantitatively, the resolution of the sensor along its optical axis, and to test its effectiveness in plotting axial profiles of the drift wave and ion acoustic wave.

Further experiments will be performed using both Langmuir and optical probe sensing units and various geometrical shapes will be tried as suppressing elements, (plate, screen, cylinders etc.), in order to allow stabilization at the lowest value of gain or power input which can be achieved.

We are also investigating a remote feedback element consisting of turns of wire around the pyrex envelope containing the arc. Fig. 23 shows some initial experimental data taken with this magnetic probe and points up its usefulness as a sensing element. This figure shows the presence of an ion acoustic wave. The magnetic coil offers advantages for use as a remote sensing element, but its feasibility as a remote suppressing element is yet to be determined.

Combinations of sensing and suppressing elements will be investigated for instabilities other than drift waves. In addition now that we have the capability of applying feedback stabilization to the plasma, quantitative investigation of the effect of growth and relative magnitude of various instabilities on plasma phenomena can proceed. With the amplitudes of coherent instabilities controlled by the feedback stabilization technique, effects on charged particle density and temperature profiles, diffusion loss rates, level of turbulence, power spectra, etc. can be studied in detail.

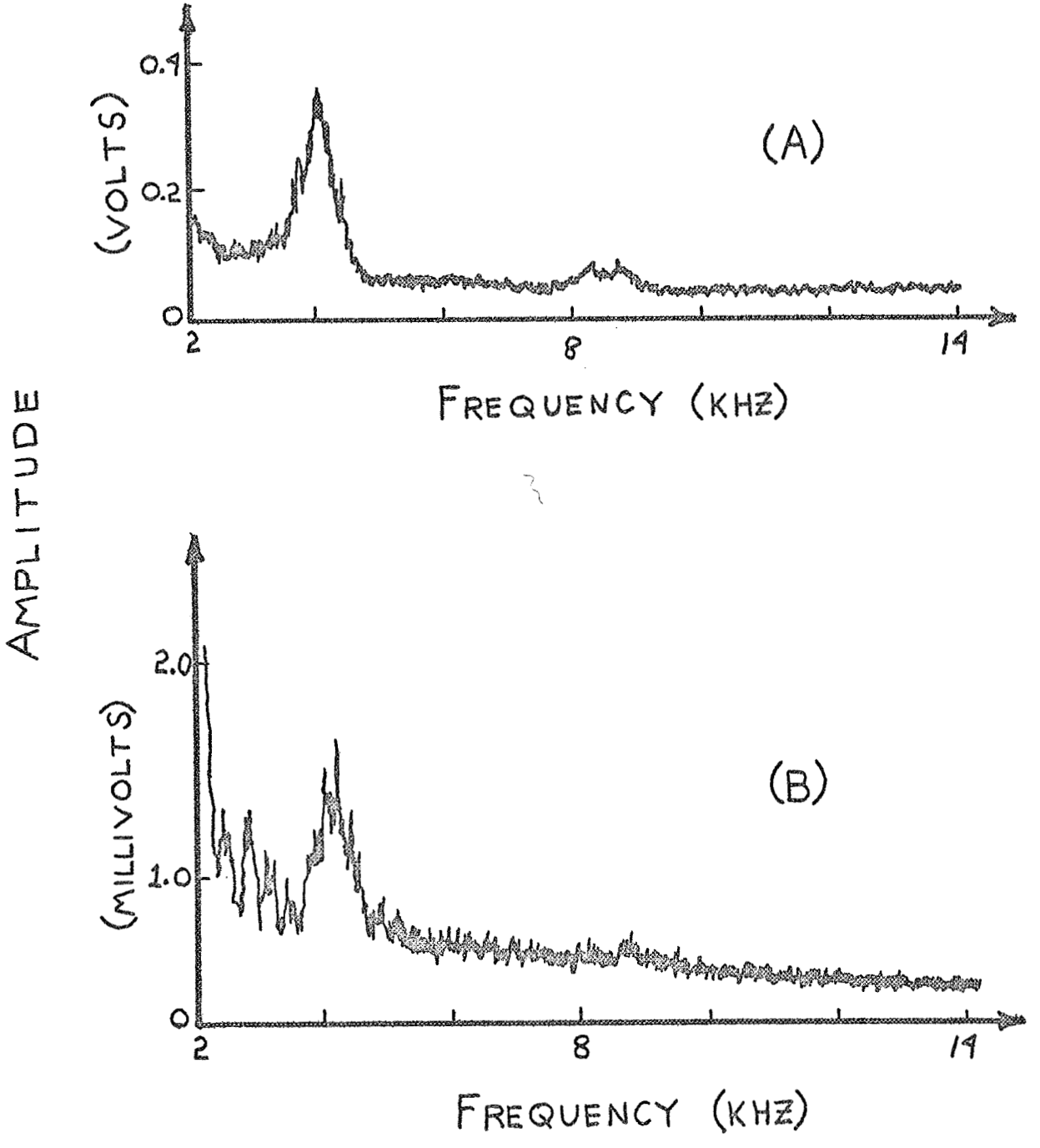

Amplitude of Ion Acoustic Wave vs. Frequency. (a) Langmuir Probe; (b) Magnetic pickup Coil.
B = 580 Gauss, P = 4.0×10^{-4} torr.

Fig 23

INSTABILITY AMPLITUDES (Theoretical)

Langmuir probe observations show that the amplitude of the driftwave instability peaks just outside the arc core, although the actual radial position of wave maximum depends on the magnetic field strength and the gas pressure. The optical probe data shows that the amplitude of the driftwave may fall to zero within the arc core. We have carried out some preliminary theoretical work which can be used to explain these experimented observations. Since further work is required, only a bried outline is included in the present report.

Invoking a fluid model in cylindrical geometry, the continuity equations for ions and electrons can be used to obtain expressions for the transverse and radial velocity components. First order perturbations in the ion density and plasma potential can then be introduced and lead to a dispersion equation, the imaginary part of which, (ω_I), is related to the wave growth rate. This expression has the following form when terms of small magnitude (appropriate to the plasma conditions in the arc) are dropped:

$$\omega_I = \frac{1}{2}\frac{\omega_{ci}^2}{\nu_{ie}}\left[\left(1 + \frac{k_z v_d}{\omega_{ci}}\left(1 - \frac{\omega_{ce}\nu_{ie}}{\omega_{ci}\nu_e}\right) - \frac{4\nu_{io}\nu_{ie}}{\omega_{ci}^2}\right)^{1/2} - 1\right]$$

where $\omega_{ci(e)}$ = the cyclotron frequency of the ion, (electron)

k_z = the axial wave number

v_d = the ion drift velocity

$\nu_{ie(o)}$ = the collision frequency between ions and electrons (neutrals)

ν_e = $\nu_{ei} + \nu_{eo}$ = the effective electron collision frequency.

Note that flute modes ($k_z = 0$) are not allowed, since finite k_z is required for wave growth. The important term affecting growth is $m_i \nu_{ie}/m_e \nu_e$, since the stability criterion involves this term, is requiring $k_z \omega_{ci} v_d (1 - m_i \nu_{ie}/m_e \nu_e) > 4 \nu_{io} \nu_{ie}$. If k_z is finite the wave will grow, provided $(m_i \nu_{ie}/m_e \nu_e) = \epsilon < 1$. However if this term ϵ is of the order of unity, and may be either positive or negative in different regions of the plasma, we can understand how onset and growth of the driftwave are affected. For a value of magnetic field B = 1500 Gauss, for example, $v_d = 10^4$ cm/sec, $\omega_{ci} = 4 \times 10^5$ sec^{-1}, so that our criterion becomes:

$$10^9 k_z \epsilon > \nu_{ie} \nu_{io}$$

In the arc k_z is of order 10^{-2}, and ϵ of order 1, so that values of order $\nu_{ie} = 10^2$ sec^{-1} and $\nu_{io} = 10^5$ sec^{-1} are required for growth. These values are not unreasonable in the highly ionized argon plasma, although magnitudes of ion collision frequencies in a magnetic field are not well known.

This simplified analysis shows how important are gradients in charged particle density and temperature, which affect the effective collision frequencies. Different radial regions of the plasma must be considered separately. In addition the phase difference between plasma potential and coherent density fluctuations must be included in a more comprehensive theoretical analysis.

Acknowledgments

The following graduate students have carried out the work reported in the preceding sections: G. Huchital, J. Stufflebeam, R. Reinovsky, and G. Kambic. The continued interest of the technical monitor, Dr. K. Thom, in this research, is gratefully acknowledged.

REFERENCES

1. Golubev, V. S., "Investigation of Charge Diffusion in Ionized Gases by the Diffusion Wave Technique", Sov. Phys. JETP 6, 1399 (1963).

2. Flannery, D. L. and Brown, S. C., "Alternating Current Diagnostic Study of Diffusion in a Highly Ionized Plasma in a Magnetic Field", Phys. Fluids 13, 1066 (1970).

3. Self, S. A. and Ewald, H. N., "Static Theory of a Discharge Column at Intermediate Pressures", Phys. Fluids 9, 2486 (1966).

4. Noon, J. H., Schmidt, H. A. and Holt, E. H., "Connection Between Self-Excited Low Frequency Oscillations and Anomalous Plasma Diffusion", Plasma Phys. 12, 477 (1970).

5. Das, K. P., "Interaction Among Three Extraordinary Waves in a Hot Electron Plasma", Phys. Fluids 14, 124 (1971).

6. Hoijer, S. and Wilhelmsson, H., "Studies of Non-Linear Resonance Conditions for Three-Wave Interactions in a Plasma", Plasma Phys. 12, 585 (1970).

7. Ogasawara, M. and Mori, S., "Sum and Difference Frequency Generation in a Plasma by Two Nonuniform Electric Fields in the Presence of a Static Magnetic Field II", J. Phy. Soc. Japan 28, 748 (1970).

8. Ohnuma, T. and Hatta, Y., "Wave-Wave Coupling in Ion Wave Propagation", J. Phy. Soc. Japan 29, 1597 (1970).

9. Ott, E., "Three Wave Mode Coupling Theory of Non-resonantly Unstable Waves", Phys. Fluids 13, 442 (1970).

10. Wilhelmsson, H., "Non-Linear Coupling of Waves in a Magnetized Plasma with Particle Drift Motives", J. Plasma Phys. 3, 215 (1969).

11. Roth, J. R., "Spectral Index and Sense of Energy Cascading in a Hot Turbulent Plasma", Bull. Amer. Phy. Soc. 15, 1427 (1970).

12. Arsenin, V. V. and Chuyanov, V. A., "Possibility of Suppressing the Drift Instability in an Inhomogeneous Plasma by a Feedback System", Atomnaya Energiya, 24, 4 (1968).

13. Keen, B. E., "Interpretation of Experiments on Feedback Control of a 'Drift-Type' Instability", Phys. Rev. Letters, 24, 6 (1970).

14. Keen, B. E. and Aldridge, R. V., "Suppression of a 'Drift-Type' Instability in a Magnetoplasma by a Feedback Technique", Phys. Rev. Letters, 22, 25 (1969).

15. Parker, R. R. and Thomassen, K. I., "Feedback Stabilization of a Drift-Type Instability", Phys. Rev. Letters, 22, 22 (1969).

16. Keen, B. E., Private Communication.

17. Aldridge, R. V. and Keen, B. E., "Rotationally Convected Drift Wave Instability in an Inhomogeneous Plasma Column", Plasma Physics, 12, (1970).

18. Chen, F. F., "Feedback Stabilization of Drift Waves by Neutral Beams", Plasma Physics Laboratory, Princeton University, 1969.

19. Chen, F. F. and Furth, H. P., "Low-Frequency Plasma Stabilization by Feedback-Controlled Neutral Beams", Plasma Physics Laboratory, Princeton University, MATT-707, 1969.

20. Chu, T. K., Hendel, H. W., Perkins, F. W. and Simonen, T. C., "Remote Feedback Stabilization of Drift Instability by Microwaves", in "Feedback and Dynamic Control of Plasmas", Chu, T. K. and Hendel, H. W., Amer. Instit. Phys., New York, 1970.

21. Chen, F. F., "Plasma Control with Infrared Lasers", in "Feedback and Dynamic Control of Plasmas", Chu, T. K. and Hendel, H. W., Amer. Instit. Phys., New York, 1970.

22. Garscadden, A. and Bletzinger, P., "Feedback Experiments on Multimode Ionization Waves", in "Feedback and Dynamic Control of Plasmas", Chu, T. K. and Hendel, H. W., Amer. Instit. Phys., New York, 1970.

23. Carlyle, C., "Passive Feedback Stabilization", in "Feedback and Dynamic Control of Plasmas", Chu, T. K. and Hendel, H. W., Amer. Instit. Phys., New York, 1970.

24. Chu, T. K., Hendel, H. W., Jassby, D. L., and Simonen, T. C., "Feedback Stabilization of the Transverse Kelvin-Helmholtz Instability - Experiment and Theory", in "Feedback and Dynamic Control of Plasmas", Chu, T. K. and Hendel, H. W., Amer. Instit. Phys., New York, 1970.

25. Simonen, T. C., "Feedback Applications to Basic Plasma Instability Experiments", in "Feedback and Dynamic Control of Plasmas", Chu, T. K. and Hendel, H. W., Amer. Instit. Phys., New York, 1970.

26. Arsenin, V. V., Zhil'tsov, V. A., Likhtenshtein, V. Kh., and Chulnov, V. A., "Suppression of Cyclotron Instability of a Rarefied Plasma with the Aid of a Feedback System", JETP Letters 8, 2 (1968).

27. Van der Pol, B., "On Oscillation Hysteresis in a Triode Generator with Two Degrees of Freedom", Phil. Mag. 43, 700 (1922).

28. Simonen, T. C., Chu, T. K., and Hendel, H. W., "Feedback Control of Collisional Drift Waves by Modulated Parallel-Electron-Current Sink--Experiment and Interpretation", Plasma Physics Laboratory, Princeton University, MATT-711, (1969).

29. Tanaca, H. and Hagi, M., "A Resonant Suppression of Low Frequency Oscillation in Plasma", J. Phys. Soc. Japan, 20, (1965).

30. Gunshor, R. L., Noon, J. H., and Holt, E. H., "Correlation Measurements of Ion Acoustic Waves in a Highly Ionized Plasma", Phys. Fluids 11, 1763 (1968).